25th International Workshop on Electromagnetic Nondestructive Evaluation (ENDE'22)

13-14 June, 2022

virtual meeting

Program and Short Papers

13 June, 2022 (Monday)

08:45 **Opening**
Sandor Bilicz, Christophe Reboud

09:00 **Analytical and numerical modeling** Chair: Antonello Tamburrino

9:00 Using Electrical Resonance in ECT: Principles, Challenges and Applications
Robert R. Hughes

9:20 Modelling of PoD Curves Incorporating Multiple Correlated Flaw Signals
Prashanth Baskaran, Artur Ribeiro, Helena Ramos

9:40 A Study on Electromagnetic Nondestructive Evaluation of Wire Breakage Rate of Superconducting Cable in CICC of Tokamak Magnet
Yinqiang Qu, Xiaochuan Liu, Xudong Li, Tianhao Liu, Wenlu Cai, Shejuan Xie, Yu Wu, Zhenmao Chen

10:00 A High Frequency Eddy Current Numerical Simulation Method Considering Dielectric Properties of Materials
Wei Guo, Shejuan Xie, Jie Han, Liang Qiao, Yali Du, Zhenmao Chen

10:20 Evaluation of Artificial Notches in Conductive Biomaterials by Sweep Frequency Eddy Current Testing
Filip Vaverka, Milan Smetana, Daniela Gombarska And Ladislav Janousek

10:40 Hybrid Model for Eddy Current Testing Defect Detection in High Frequencies
Athanasios Kyrgiazoglou, Theodoros Theodoulidis

12:00 **Inverse problems, imaging and signal processing** Chair: Dominique Lesselier

12:00 A gradient-improved particle swarm optimizer using surrogate modeling
Charles Boulitrop, Marc Lambert, Sándor Bilicz

12:20 A Micro EIT Sensor for Real-Time and Label Free Biological Imaging
Antonello Tamburrino, Antonio Affanni, Ruben Specogna, Francesco Trevisan

12:40 Wireless RF Multifrequency Resonator for the Non-invasive Monitoring of Tumors in Breast Tissues
Alexiane Pasquier, Yohan Le Diraison, Stephane Serfaty, Pierre-Yves Joubert

13:00 Data fusion and non-destructive testing of damaged fiber-reinforced laminates
Valentin Noël, Thomas Rodet, Dominique Lesselier

13:20 Tomography of Nonlinear Magnetic Materials via the Monotonicity Principle
Antonello Tamburrino, Antonio Corbo Esposito, Luisa Faella, Vincenzo Mottola, Gianpaolo Piscitelli, Ravi Prakash

13:40 Monotonicity based Imaging Method using Time-Domain Eddy Current Measurements
Antonello Tamburrino, Zhiyi Su, Lalita Udpa, Gianpaolo Piscitelli

14 June, 2022 (Tuesday)

09:00 **Advanced sensors** Chair: Christophe Reboud

9:00 Efficient design of remote field eddy current array probe for imaging of defects in small diameter ferromagnetic tube
Thulasi Vijayachandrika, S. Thirunavukkarasu, Anish Kumar

9:20 Small Diameter Array Probe with TMR Sensors and Elliptical Excitation for Thimble Tube Inspection
Jingyi Wang, Xinchen Tao, Chaofeng Ye

9:40 Eddy current sensor interface from frequency output sensors to LDC based integrative eddy current test
Guiyun Tian, Xiaolong Lu

10:00 **Non-destructive Testing and Evaluation** Chair: Guiyun Tian

10:00 Purpose and Practical Capabilities of the Metal Magnetic Memory Method
Sergey Kolokolnikov, A.A. Anatoly Dubov, Péter Ladányi

10:20 Probability of detection considering both the depth and circumferential length of pipe wall thinning using microwave NDT
Yijun Guo, Takuma Tomizawa, Noritaka Yusa, Hidetoshi Hashizume

10:40 Hardware and Software Design for a Battery-powered Portable Pulsed Eddy Current (PEC) System
Xiong Lei, Zihan Xia, Ruochen Huang, Jialong Shen, Wuliang Yin

11:00 Scattering Matrix-based Dielectric Permittivity Estimation of Bulk Materials
Botond Tamas Csatho, Csaba Endre Berky, Balint Peter Horvath

12:00 **Complex material characterization** Chair: József Pávó

12:00 Identification of constitutive parameters of ferrite cores in common mode chokes
Balint Pinter, Arnold Bingler, József Pávó

12:20 Quality control of thermal and thermochemical treatment on mechanical components by electromagnetic methods
Hélène Petitpré, F. Zhang, N. Samet, E.b. Ndiaye, S. Bonnin, S. Chomer, C. Gallais, L. Gautier

12:40 Modelling of carbon fibre composite structures using high-frequency eddy current imaging
Qiuji Yi, Paul Wilcox, Robert R. Hughes

13:00 Electromagnetic Methodology for Mechanical Stress Evaluation of Anisotropic Ferromagnetic Materials
Safae Bouterfas, Yann Le Bihan, Laurent Santandrea And Laurent Daniel

13:20 Measurement and Modelling Magnetic Anisotropy due to Crystallographic Texture in Interstitial Free (IF) Steels
Mohsen Aghadavoudi Jolfaei, Jun Liu, Frenk van Den Berg, Claire Davis

13:40 Effects of Tensile and Comprresive Stress on Magnetic Parameters of Martensitic Stainless Steel
Hiroaki Kikuchi, Kohei Sugai, Keiichi Matsumura

14:00 Mechanical stress estimation through classical and magnetic Barkhausen noise energy hysteresis cycle
Patric Fagan, Anastasios Skarlatos, Chrisophe Reboud, Laurent Daniel, Mathieu Domenjoud, Benjamin Ducharne

Using Electrical Resonance in ECT: Principles, Challenges and Applications

Robert R. HUGHES [a,1]
[a] *CAME School of Engineering, University of Bristol, UK*

Abstract. Electrical resonance is seen as a nuisance by many when designing & performing eddy-current testing (ECT) inspections**.** Tricky to model and difficult to control, it is regularly avoided, but research has shown that it can be used to improve the signal-to-noise to material features and could open the door for novel sensor systems. In this paper, the author summarises work conducted in this area, presenting research on the principles and modelling of resonant behavior in ECT inspections, and discusses the potential applications and challenges of resonance-based techniques for non-destructive testing.

Keywords. ECT, Eddy-Currents, Resonance.

1. Introduction

The exploitation of electrical resonant behavior is not a new approach in eddy-current testing (ECT). Some of the earliest analogue ECT systems exploited the large amplitude changes that occur around electrical resonance of eddy-current coils when in the presence of changes in lift-off, defects and material features [1]. However, as technology developed, and digital systems allowed for greater control and quantitative evaluation, the instabilities of resonance were deemed too problematic to account for, leading to the abandonment of resonance-based methods in favour of more stable, easy to model sub-resonance excitation techniques [2]. In doing so, any benefits of resonance have been forgotten.

Despite this, there are still advantages to employing electrical resonance in certain ECT applications. Over the last few decades the exploitation of shifting behaviour in electrical resonance has reemerged in ECT research as a means of enhancing the sensitivity of inspections [3]–[6]. Research into this effect indicates that resonance-based sensing could be a powerful tool in the ECT measurement arsenal, exhibiting higher signal-to-noise ratios to material features [7],. However, without an adequate understanding and robust models for resonant behavior, techniques exploiting resonance will remain a fringe research practice.

In this paper, the research conducted to date on the characterisation and modelling of resonance-based eddy-current sensing is summarized and discussed, with a focus on the potential applications, practical limitations and future challenges.

Analytical expressions, derived from circuit theory, for the critical features of electrical resonance, including resonant frequency, peak amplitude and full width half maximum were examined, and their predictive powers compared to other methods of

[1] Robert R. Hughes, Department of Mechanical Engineering, University of Bristol, Queen's Building, University walk, Bristol, BS8 1TR, UK; E-mail: Robert.hughes@birstol.ac.uk

modelling resonance developed [8]. Accurate resonant spectra models were developed using genetic (differential evolution) algorithms to optimize unknown variables in the multi-dimensional parameter space [9]. These models are then used to test simple predictive models simulating the effect of defects on resonance and compared to experimental resonant spectra measurements, recorded using a low MHz range impedance analyser, of wire-cut slots and EDM notches in Aluminum. The circuit model and experimental data are then compared to bespoke 2D & 3D finite element analysis (FEA) models, developed in COMSOL, and used to invert rectangular notch defect dimensions.

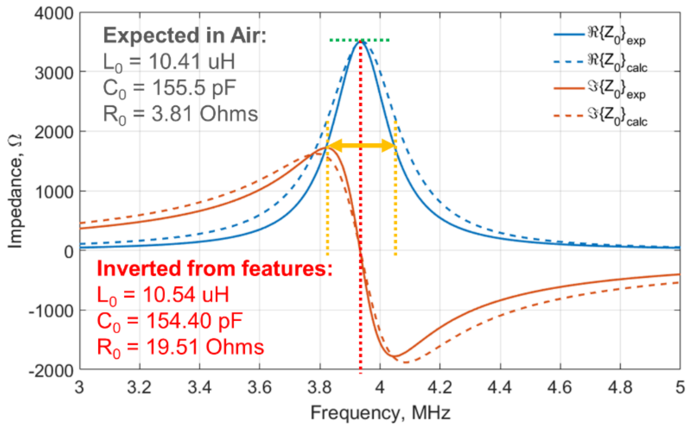

Figure 1. Modelled resonant spectra: Circuit model (dashed) verses experimental (solid), giving inverted values calculated from measured resonant features.

References

[1] C. N. Owston, "A high frequency eddy-current, non-destructive testing apparatus with automatic probe positioning suitable for scanning applications," *J. Phys. E-Scientific Instruments*, vol. 3, no. 10, pp. 814-, 1970, doi: 10.1088/0022-3735/3/10/317.

[2] M. Gal-Katziri and A. Hajimiri, "Analysis and Design of Coupled Inductive Bridges for Magnetic Sensing Applications," *IEEE J. Solid-State Circuits*, vol. 54, no. 7, pp. 1883–1894, Jul. 2019, doi: 10.1109/JSSC.2019.2907196.

[3] R. T. Ko, M. P. Blodgett, S. Sathish, and T. R. Boehnlein, "Resonant Frequency Eddy Current Liftoff Measurements for Shot Peening Intensity Assessment in Materials (Preprint)," 2007.

[4] R. Bossi *et al.*, "Advanced Nondestructive Evaluation ({NDE}) Sensor Modeling For Multisite Inspection." 2008.

[5] J. M. Kim *et al.*, "An Effective Electrical Resonance-Based Method to Detect Delamination in Thermal Barrier Coating," *J. Therm. Spray Technol.*, vol. 27, no. 3, pp. 336–343, Feb. 2018, doi: 10.1007/s11666-017-0670-2.

[6] C. Y. Liu and Y. G. Dong, "Resonant Coupling of a Passive Inductance-Capacitance-Resistor Loop in Coil-Based Sensing Systems," *IEEE Sens. J.*, vol. 12, no. 12, pp. 3417–3423, 2012, doi: 10.1109/jsen.2012.2190057.

[7] R. R. Hughes and S. Dixon, "Performance analysis of single-frequency near electrical resonance signal enhancement (SF-NERSE) defect detection," *NDT E Int.*, vol. 102, pp. 96–103, Mar. 2019, doi: 10.1016/j.ndteint.2018.11.008.

[8] R. R. Hughes and S. Dixon, "Analysis of electrical resonance distortion for inductive sensing applications," *IEEE Sens. J.*, 2018, doi: 10.1109/JSEN.2018.2841506.

[9] R. R. Hughes and B. W. Drinkwater, "Exploring high-frequency eddy-current testing for sub-aperture defect characterisation using parametric-manifold mapping," Feb. 2021.

Modelling of PoD Curves Incorporating Multiple Correlated Flaw Signals

Prashanth BASKARAN [a,1], Artur RIBEIRO [a] and Helena RAMOS [a]

[a] *Instituto de Telecomunicações, Instituto Superior Técnico, Universidade de Lisboa, Lisboa, Portugal*

Abstract. Probability of detection (PoD) models take into consideration one or multiple flaw parameters, say the length, maximum depth, or surface area, and a single flaw signal. However, due to the correlation between the response signals, it might be necessary to consider multiple response signals to know about the flaw. Hence, in this work, we demonstrate the possibility of including multiple correlated flaw signals (features) towards the construction of a PoD curve. The flaw features considered are the peaks of the 3 components of the magnetic flux density i.e. B_x, B_y, and B_z. This is a fully model assisted (FMA) study in which an aluminium plate, that contains a narrow opening flaw, is inspected by an eddy current probe that induces spatially uniform fields in the conductor in the region of interest. The analysis was performed using the semi-analytical boundary element method.

Keywords. Boundary element method, Magnetic flux density, Model assisted PoD

1. Problem Motivation and Boundary Element Analysis

Probability of detection (PoD) study, of a specific method, aims at determining the probability at which a flaw of certain dimensions is detectable. These studies are necessary in an industrial context because the NDT inspectors are viable to make imperfect inspections and may miss the detection of a fatal flaw. Conventional PoD study involves considering just one flaw parameter, say the flaw length or depth, and one flaw signal, say the peak of the induced voltage, the magnetic flux density components measured by a sensor or the coil impedance. However, some studies have indicated that multiple flaw parameters are needed to accurately evaluate PoD [1]. Another study indicated that multiple flaw features are needed to evaluate cracks as they may provide complimentary informations. Hence, multiple flaw parameters and signals are needed to make a more reliable PoD study. Thus, it is necessary to perform a PoD study that can integrate multiple flaw features, which is the aim of the current study.

In this work, we have considered flaws with rectangular cross-section located in the sub-surface of a 5 mm thick aluminium plate whose electrical conductivity is $\sigma = 14.6$ MSm^{-1}. The excitation coil considered for the test is an uniform eddy current probe that induces a uniform field in a small region, along x axis, where the three components of the magnetic flux density B_x, B_y, and B_z are evaluated.

[1] Corresponding Author: E-mail: prashanth.baskaran@tecnico.ulisboa.pt

Due to the consideration of a narrow opening flaw, it can be modelled as a secondary source which is populated by electric dipoles that are oriented normal to the flaw surface opposing the incident electric field. In order to determine the scattering field i.e., the fields produced by the electric dipole sources, it is necessary to know the distribution of the dipole density. The scattering fields are generally modelled as an integral equation, involving the Green's function of appropriate type. Applying the boundary condition of vanishing normal component of the electric field to the flaw and invoking the method of moments, it is possible to convert the integral equations to a linear form and then determine the electric dipole density in the discretized flaw domain. Using the magnetic-electric Green's functions in air [2], it is possible to determine the perturbed magnetic field components.

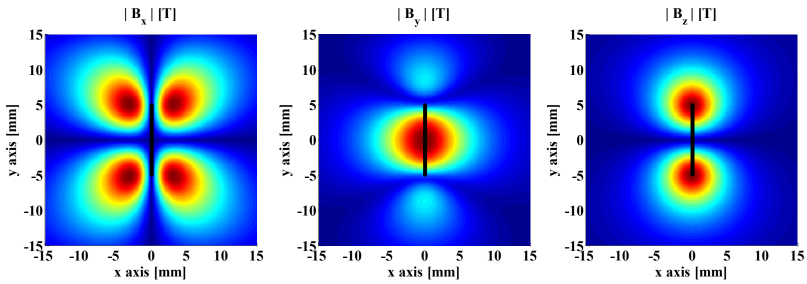

Figure 1. Scattering of (a) $|B_x|$, (b) $|B_y|$, and (c) $|B_z|$ due to a sub-surface flaw, located at the center.

2. PoD model and Discussion

The PoD model is performed for varying flaw lengths and depths and the flaw features being the peak of the magnetic field components. To simulate the effect of noise, lift-off variations have been considered. Hence for a given flaw case, we have a distribution of the features. We fit it with a Gaussian function and then compute the PoD by fixing the detection threshold. From the discrete form of PoD, we fit it with a generalized logistic function to obtain the PoD curve [2]. This kind of modelling integrates several correlated flaw parameters (flaw length and depth) and features (peak of B_x, B_y, andB_z).

Acknowledgment

This work was developed at Instituto de Telecomunicações (IT) and was supported by the Portuguese Science and Technology Foundation, projects UIDB/50008/2020 and PTDC/EEI-EEE/30723/2017.

References

[1] Noritaka Yusa, Weixi Chen, Hidetoshi Hashizume, Demonstration of probability of detection taking consideration of both the length and the depth of a flaw explicitly, *NDT & E International* **81** (2016).

[2] Prashanth Baskaran, D.J. Pasadas, A.L. Ribeiro, H.G. Ramos, Probability of detection modelling in eddy current NDE of flaws integrating multiple correlated variables, *NDT & E International* **123** (2021).

A Study on Electromagnetic Nondestructive Evaluation of Wire Breakage Rate of Superconducting Cable in CICC of Tokamak Magnet

Yinqiang Qu[1], Xiaochuan Liu[2], Xudong Li [1], Tianhao Liu [1], Wenlu Cai [a,2], Shejuan Xie[1], Yu Wu[2], Zhenmao Chen [1,*]

[1] State Key Laboratory for Strength and Vibration of Mechanical Structures, Shaanxi Engineering Research Center for NDT and Structural Integrity Evaluation, Xi'an Jiaotong University, Xi'an, 710049, China

2. Institute of Plasma Physics, CAS, Hefei 230031 China

Abstract. The wire broken rate exceeding the threshold value may cause quench problem in superconducting magnet using cable in conduit conductors (CICC), which is one of the big concerns of the safe operation of a superconducting Tokamak nuclear fusion device. Based on the DC potential drop (DCPD) method and the DC magnetic field measurement (DCFM) method, nondestructive testing techniques of wire breakage state are studied through numerical analyses and experiments. At first, a transverse isotropic numerical code for direct current conducting problem of the superconducting cable is developed and the signals of potential drop at the cable surface and the magnetic field surrounding the cable are calculated. Second, the influence of broken wire rate and position of defect on the inspection signals are investigated based on the numerical results. The numerical results reveal that the signal features of both the DCPD and DCFM signals have good potential to characterize the state of wire breakage. Finally, experimental systems for DCPD and DCFM are established and measurements of CICC test-pieces with artificial defects are conducted. The experimental results verified the feasibility of the both methods for the nondestructive testing of the wire breakage of superconducting cables.

Keywords. Wire breakage detection, Transverse isotropic, DC potential drop method, DC magnetic field measurement method

1. Introduction

The development of controllable nuclear fusion technology can make the peaceful utilization of fusion nuclear energy possible, as well as solve the sustainable development problem of human beings. The Tokamak device based on the magnetic confinement is considered to be the most likely way to realize the controllable nuclear fusion. One of the key components of the Tokamak device is the superconducting magnet, and it is twining made by superconducting cable-in-conduit-conductor (CICC). The

* Corresponding Author, Xi'an Jiaotong University, China; E-mail: chenzm@mail.xjtu.edu.cn

CICC is internally consist of superconducting wires, which is tightly twisted together during fabrication procedure, and improper procession may cause damage to superconducting wires [1]. When the wire broken rate exceeds the threshold value, it may cause quench problem during operation and threaten the safety of whole Tokamak device. Therefore, it is significant to develop a nondestructive testing method to detect and evaluate the wire breakage rate of the superconducting cable.

2. Method and Results

The DC potential drop method (DCPD) has no skin effect and the current can flow into the test-pieces which makes it sensitive to inner defect in inspection target [2]. On the other hand, the DC magnetic field measurement (DCFM) also can detect the inner defects but without direct contacting measurement. The aim of this study is to explore the feasibility of these two methods for wire breakage detection through numerical simulation and experiments, in order to find a better way for practical inspection.

In practice, a numerical code based on a transverse isotropic conductivity model are developed for simulation of conducting current in the superconducting wire and the corresponding DCPD and DCFM signals based on a conventional 3D FEM code. The signals perturbation of the potential drop at the cable surface and the magnetic field surrounding the cable due to artificial wire breakage defect of different size are then calculated. Through feature analyses of the simulated signals, the detectability and the sensitivity of the two NDT methods are compared in view of detection and quantitative evaluation of wire breakage in CICC. Finally, an experimental system is established, and the detectability of the DCPD and DCFM techniques for defects in CICC is investigated experimentally.

Fig.1 gives a typical simulation results of the DCPD and DCFM signals for a surface wire breakage of 3%. It is clear that the defect causes a significant signal perturbation, which reveals a good possibility to apply these techniques for NDT of defects in CICC. The numerical results also show that the signal amplitude and distribution also have clear correlation with the defect size and location. In addition, the experimental results show the same tendency with the numerical simulation results, and verified the effectiveness experimentally. Details will be given and discussed in the full paper.

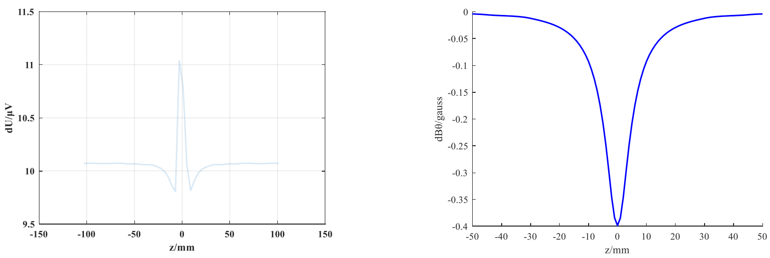

Fig.1 Typical DCPD and DCFM simulation signals for a 3% wire breakage defect

References

[1] Qin J G, Wu Y, Liao G, et al. Cable rotation and twist pitch variation for ITER TF conductor in China. IEEE Trans. Applied Supercond., 2014, 25(3): 1-4.

[2] X. Wang, S. Xie, Z. Chen, An Efficient Numerical Scheme for Sizing of Cavity Defect in Metallic Foam From Signals of DC Potential Drop Method. IEEE Trans. Magn., 2014, 50(2): 125-128.

A High Frequency Eddy Current Numerical Simulation Method Considering Dielectric Properties of Materials

Wei Guo, Shejuan Xie*, Jie Han, Liang Qiao, Yali Du, Zhenmao Chen*
[1] *State Key Laboratory for Strength and Vibration of Mechanical Structures, Shaanxi Engineering Research Center for NDT and Structural Integrity Evaluation, Xi'an Jiaotong University, Xi'an 710049, China*
Corresponding authors: chenzm@xjtu.edu.cn

Abstract. Conventionally, the displacement current is ignored in numerical simulation of Eddy Current Testing (ECT) signals as its frequency is usually relative low. How is the effect of dielectric property on high frequency ECT for inspection of CFRP material is not clear. In this paper, a numerical method for high frequency ECT is proposed and implemented. A 3D ECT forward solver based on the FEM-BEM hybrid method is developed with the displacement current taken into account. Based on the developed numerical code, the influence of electric conductivity and permittivity on high frequency ECT signals is studied numerically and found the dielectric property has to be considered when frequency is higher than 200 MHz.

Keywords. High frequency eddy current, 3D solver, dielectric property

1. Introduction

Eddy current testing (ECT) is a widely used NDT method with advantages of non-contact, rapid inspection speed and high detectability for surface and near surface defect [1]. Conventionally, the excitation frequency of ECT is usually lower than 1 MHz, which enables the displacement current to be ignored in ECT simulation as it is far less than the value of eddy current. However, the low frequency assumption makes the conventional ECT forward solver not applicable for the high frequency eddy current problems, which is becoming important for inspection of defect in CFRP material.

To develop numerical method for the high frequency ECT problem, the A-ϕ governing equation for conventional ECT problem was updated with the displacement current term taken into account in the Maxwell equations. Then, a 3D numerical code was developed for the high frequency ECT problem based on deduced governing equations and the FEM-BEM hybrid discretization. With the developed code, the influence of electric permittivity on ECT signal was studied numerically.

2. High frequency ECT simulation with consideration of displacement current

High frequency eddy current field governing equation in A-ϕ form are as follows:

$$\begin{cases} \dfrac{1}{\mu}\nabla^2\widetilde{\boldsymbol{A}} = \widetilde{\sigma}\left(\dfrac{\partial\widetilde{\boldsymbol{A}}}{\partial t} + \nabla\widetilde{\phi}\right) \\ \nabla\cdot\widetilde{\sigma}\left(\dfrac{\partial\widetilde{\boldsymbol{A}}}{\partial t} + \nabla\widetilde{\phi}\right) = 0 \end{cases} \tag{1}$$

where $\boldsymbol{A}$ is the magnetic vector potential, ϕ is the scalar potential, μ is the relative permeability, $\widetilde{\sigma} = \sigma + j\omega\varepsilon$ is complex conductivity with consideration of permittivity. Eqs. (1) have just the same form with the governing equations of the low frequency ECT problem, therefore it can be discretized and solved with the FEM-BEM method [2].

3. Effect of permittivity on eddy current testing signals

By using the developed ECT simulator with and without considering the dielectric effect, S_c, ECT signals without considering displacement current and S_d, ECT signals with considering the displacement current were calculated. In Fig. 1a, numerical results on relative change of signals with and without considering the dielectric effect is given. In case of 1 GHz frequency and low conductivity, the relative signal change may reach as large as 30%. Fig. 1b and Fig. 1c show the simulated ECT signals and relative error for different frequency when conductivity is 10 S/m. If we define that the influence is obvious when the relative error is larger than 1%, we can conclude based on the numerical results that the dielectric effect is not negligible when frequency is larger than 200 MHz.

4. Conclusion

In this paper, a numerical method and related code for high frequency ECT problem is developed based on the FEM-BEM hybrid method and taking the dielectric effect into account. The dependence of the ECT signals on the frequency and displacement current is investigated numerically with the developed code.

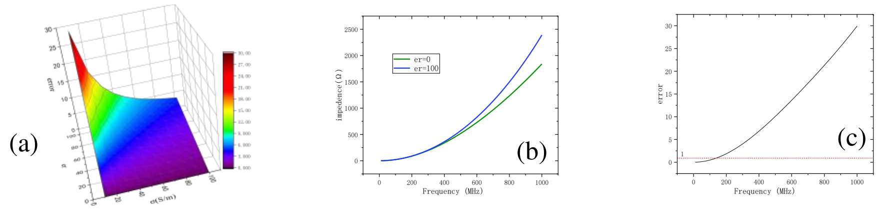

Figure 1. Numerical results for high frequency ECT problem a) Signal at 1 GHz, b) Swept-frequency signal c) relative error

References

[1] Z. Chen, C. Jomdecha, S. Xie, Eddy Current Testing, in Handbook of advanced NDE, eds. N. Ida, N. Meyendorf, Springer, Cham, 2019.

[2] Z.Chen, N.Yusa, K.Miya, Some advances in numerical analysis techniques for quantitative ENDE, NDTE, Vol.24, 69-102, 2009

Evaluation of Artificial Notches in Conductive Biomaterials by Sweep Frequency Eddy Current Testing

Filip VAVERKA, Milan SMETANA, Daniela GOMBARSKA and Ladislav JANOUSEK

Department of electromagnetic and biomedical engineering, Faculty of Electrical Engineering University of Zilina
Zilina, Slovak Republic

Abstract. The article deals with the utilization of the sweep frequency eddy current technique as an innovative method for material defect evaluation. The new eddy current probe is designed and presented. The sensitivity and the resolution of the probe, in contrast with the lift-off parameter, are investigated numerically. The simulation results are carried out while the harmonic signal is used for the driving of the eddy-current probe. The results will be presented and discussed in the full paper.

Keywords. Conventional eddy current testing, sweep-frequency eddy current testing, artificial notches, eddy-current probe.

1. Introduction

A wide spectrum of non-destructive methods for detecting inhomogeneities are currently known. Many of these techniques are based on ultrasonic, radiographic, electromagnetic, and optical principles. One such method is eddy current testing (ECT). The ECT idea is based on the electrical induction of currents in electrically conductive materials. Induced eddy currents create a secondary magnetic field, which interacts with the probe's main magnetic field. The presence of material defects disturbs the eddy currents and thus alters the probe's magnetic flux density. Maximum values of eddy currents, as well as magnetic flux, are at the material surface. As the depth increases, they slowly attenuate and lag in phase. This phenomenon is known as the skin effect and the phenomenon depends on operating frequency, material permeability, and conductivity. In eddy current inspection the most common technique is the single-frequency ECT (so-called conventional approach), pulsed, chirp ECT, etc. In the first case, a single frequency sinusoidal signal excites the coil. In the second case, the coil is excited by a square-shaped signal. In both techniques, the depth of the penetration may not be sufficient for detecting profound defects due to the skin effect. They can also suffer from errors due to distance variations between the sensor and the test object, known as the lift-off effect. [1] [2]

The optimal depth of penetration depends on conductivity, permeability, and excitation frequency. As a result, those parameters must be set very precisely. However, the change of conductivity or permeability of the material is not feasible. Furthermore, determining the appropriate frequency of simulation is quite difficult. Therefore, the use of sweep frequency eddy current testing (SFECT) has been introduced. SFECT works with a wide range of frequencies and does not need the selection of only one or two frequencies.

2. Numerical simulation of SFECT: procedure and results

This work aims to simulate the reliability of defect detection in reliance on lift-off parameter. SFECT technique is used for all the simulations. The frequency interval ranges from 1 kHz to 100 kHz within the 1 kHz step. The model designed for the simulation model consists of the metal plate of austenitic stainless steel. The plate model is a square-shaped body with an edge with a length of 200 mm and a height of 10 mm. The electromagnetic properties of the material used in the model are relative permeability $\mu_r = 1$ and conductivity $\sigma = 1.35$ MS.m^{-1}. The artificial defect is positioned in the center of the plate, with a thickness of 0.2 mm and a length of 10 mm. The depth of the defect varies from 1mm to 9 mm within a 2 mm step. The probe model is represented by a system of two independent coils: the transmitting and the receiving coil that are connected independently. The transmitting coil is supplied with a harmonic excitation voltage of $V = 100$ mV. The lift-off dependency is measured at 0.5, 1.0, 1.5, 2.0, 2.5, 3.0 mm of the probe from the surface of the material. All measured responses of the receiving coil are plotted, analyzed, and discussed. The current density field in the material is also examined. The simulation result for frequency 1 kHz with lift off 0.5 and defect depth 1 mm is shown in Figure.1.

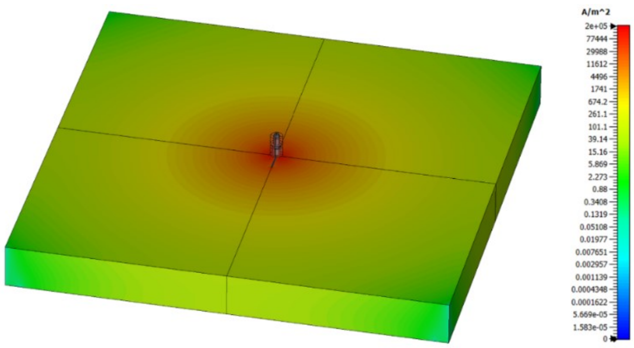

Figure 1. Numerical simulation result: current density at frequency of f =1 kHz

References

[1] B.P.C. Rao, *Practical eddy current testing*, Alpha industries International Ltd., Oxford United Kingdom., 2007.

[2] W.Yin, Thickness measurement of non-magnetic plates using multi-frequency eddy current sensors, *NDT & E International* **40** (2007), 43-48.

Hybrid Model for Eddy Current Testing Defect Detection in High Frequencies

Athanasios KYRGIAZOGLOU[a,1] and Theodoros THEODOULIDIS[a]

[a] *Department of Mechanical Engineering, University of Western Macedonia, Bakola & Sialvera, Kozani 50132, Greece*

Abstract. In this paper we present a modification of an existing analytical model for a long surface crack on a conductive plate. This is actually a thin skin model and the challenge for its successful implementation is the accurate calculation of the magnetic field on the defect-free surface on a conductor. We can now combine analytical expressions with numerical results to calculate the coil impedance changes, due to the defect existence. Using the numerical results by FEM for the coil's magnetic field into the final impedance change analytical expression we can simulate eddy current probes with complex shape that are difficult to describe analytically.

Keywords. Eddy Current Testing, hybrid model, non-destructive testing, FEM, analytical calculations.

1. Introduction

Eddy current testing (ECT) is applicable to surface crack inspections for high frequencies and a negligible crack opening. A discontinuity affects the eddy current flow, which in turn changes the coil impedance. Analytical modelling of discontinuities, that simulate defects, can be used in order to simulate such ECT inspections. A relatively accurate model for the ECT inspection is the model developed by Harfield and Bowler, which is valid for high frequencies [1]. This model uses the magnetic field on the surface of a conductive plate. The Harfield and Bowler model can be simplified by modifying some of the coefficients and moreover it implements the simplest version of a long crack [2].

In this paper we present a modification of this thin-skin model for a long crack, combining the analytical code solution with numerical results from a finite element method software, COMSOL ® Multiphysics in order to compute the coil impedance change. The idea is to numerically compute the magnetic field once with FEM. As a result, we expand the scope of the model to complex probe shapes that cannot be described analytically.

[1] Corresponding Author, Athanasios Kyrgiazoglou, Department of Mechanical Engineering, University of Western Macedonia, Bakola & Sialvera, 50132 Kozani, Greece; E-mail: akyriazoglou@uowm.gr.

2. ECT Calculation

From the existing analytical model, the expression for the coil impedance change is provided with respect to the long crack coefficients and the coil magnetic potential along the surface crack line.

$$\Delta Z = \frac{\mu_0 \omega}{2\pi} \int_{-\infty}^{\infty} \frac{g}{1 + 2(v / jk)\tilde{U} \tanh(vb)} \tilde{\varphi}^{(i)}(-v) \tilde{\varphi}^{(i)}(v) dv \tag{1}$$

where g is a coefficient that describes the defect and $\tilde{\varphi}^{(i)}$ is the Fourier transform of magnetic potential (with respect to defect's parallel axis). The magnetic potential $\varphi^{(i)}$ is defined by $\mathbf{H}^{(i)} = \nabla \varphi^{(i)}$ where $\mathbf{H}^{(i)}$ is the unperturbed magnetic field at the crack line in the absence of the crack and in Fourier transform it is written as $\tilde{H}_y^{(i)} = jv\tilde{\varphi}^{(i)}$. The main idea is to use the numerical results for the magnetic field H_{FEM} to compute the $H_y^{(i)}$.

3. Results

Fig.1 shows results for air core and ferritic core square coils above a long surface defect in non-ferromagnetic conductive thick plate.

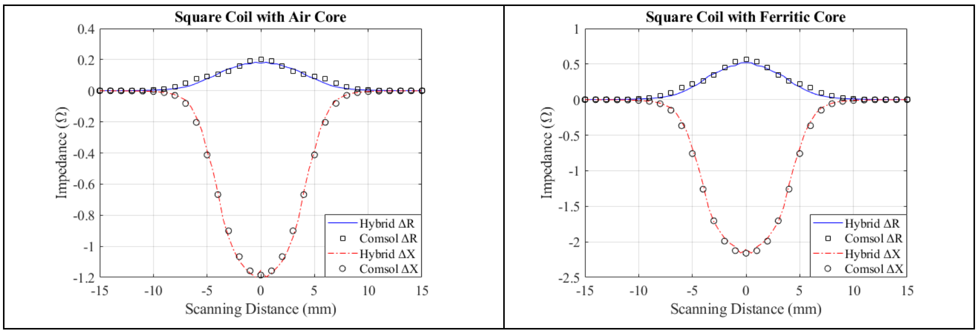

Fig. 1: Impedance Components for air core (Left) and ferritic core (Right) square coils as a function of scanning distance.

The hybrid model compares well to FEM simulation results and in addition it is many times faster, actually the time required for a full scan of the hybrid model is comparable to the time required by FEM only for one coil's position.

References

[1] N. Harfield, J.R. Bowler, Theory of thin-skin eddy-current interaction with surface cracks, *Journal of Applied Physics* **82** (1997), https://doi.org/10.1063/1.366196, 1997.

[2] T. Theodoulidis, E. Kriezis, Eddy Current Canonical Problems (with applications to nondestructive evaluation), *TechScience Press,* USA, 2006.

A gradient-improved particle swarm optimizer using surrogate modeling

Charles BOULITROP, [a,1] Marc LAMBERT [a] and Sándor BILICZ [b]

[a] *Université Paris-Saclay, CentraleSupélec, CNRS, Laboratoire de Génie Electrique et Electronique de Paris, 91192, Gif-sur-Yvette, France.*
Sorbonne Université, CNRS, Laboratoire de Génie Electrique et Electronique de Paris, 75252, Paris, France

[b] *Department of Broadband Infocommunications and Electromagnetic Theory*
Budapest University of Technology and Economics
3 Muegyetem rkp, H-1111 Budapest, Hungary

Abstract. An optimization scheme combining a PCE metamodel and a PSO optimizer has been implemented and tested on both a well-posed and an ill-posed ECT configuration. The algorithm has been improved by integrating the information of the gradient of the PCE, improving the quality of the parameter retrieval.

Keywords. inverse problems, particle swarm optimization, surrogate modeling, polynomial chaos expansion

Introduction Inverse scattering problems can be solved by using optimization, in which a cost function is minimized. The cost function usually measures the misfit between observations and simulations computed with the sought parameters. However, the computational weight of running such an optimization with an exact physical solver can often be computationnally demanding. Metamodels – or surrogate models – aim at replacing the exact physical solver by an approximate mathematical function that describes the physical solver over the search space. This improves the optimization by avoiding to solve the physical problem at each iteration, at the cost of building a set of solutions to the problem over the search space beforehand [1].

Method A Polynomial Chaos Expansion (PCE) is used to surrogate the physical solver. The UQLab toolbox [2] is used to compute the coefficients of the expansion. The main advantage of the PCE metamodeling framework is its closed-form expression, from which its gradient can be computed.

The PCE metamodel is integrated inside a Particle Swarm Optimizer (PSO). The PSO is a stochastic iterative global optimization algorithm, based on the social behavior of groups of animals [3]. A swarm of particles explores the search space, which is mapped by a cost function. Thanks to the gradient of the metamodel [4], the gradient of the cost function is computed and used to increase the speed of convergence towards the minimum of the cost function [5].

Configurations The designed method has been tested over two Eddy Current Testing (ECT) configurations. The first one, from an internal L2S-ELEDIA collaboration [6], has a single rectangular crack with varying depth, length and width. It is made of 1000 points sampled as a uniform grid in the 3-dimensional search space. The second one, from the JSAEM [7], has two rectangular cracks with varying depths, lengths and separation gap between them. It is made of 500 points sampled by Latin Hypercube Sampling (LHS) over the 5-dimensional search space. This problem tends to be ill-posed, since for small values of the separation gap, very similar impedance maps correspond to different flaw configurations.

[1] Corresponding Author E-mail: charles.boulitrop@geeps.centralesupelec.fr

Results To assess the performance of the optimization, the retrieved parameters are compared to their expected values, which gives a measure called reconstruction error. The reconstruction error between a reconstructed set of parameters $\widehat{\mathbf{X}}^*$ and the expected set of parameters $\mathbf{X}^*$ is given by $\mathrm{E} = \frac{1}{d}\sum_{i=1}^{d} |\widehat{\mathbf{X}}_i^* - \mathbf{X}_i^*|$ where d is the dimension of the search space and $|.|$ is the absolute value over $\mathbb{R}$.

The gradient-improved PSO performed better than the PSO alone both in terms of mean and variance of reconstruction error. However the gradient step size computation made it run much slower. Table 1 summarizes these results. The computations have been carried out on an Intel® Xeon® E5-2660, with 2 CPUs, 16 cores each at 2.20 GHz clock speed.

Number of parameters	Algorithm	Computation time (s)	norm. reconstruction error Mean	Std
3	PSO	0.46	98.76×10^{-3}	150.8×10^{-3}
	GPSO	4.80	74.02×10^{-3}	82.12×10^{-3}
5	PSO	9.07	202.6×10^{-3}	356.5×10^{-3}
	GPSO	191.57	140.7×10^{-3}	305.4×10^{-3}

Table 1. Comparison of reconstruction errors of the two algorithms on the two configurations

Conclusion and further works The integration of a PCE metamodel inside a particle swarm optimizer has been studied and tested over two ECT configurations, yielding good results. Additionnally, the proposed method has been refined by adding a local search thanks to the information of the gradient of the metamodel.

The current algorithm could be used for sensitivity analysis, and a solution to ill-posedness could be of interest.

References

[1] S. Ahmed et al., "An adaptive sampling strategy for quasi real time crack characterization on eddy current testing signals", *NDT & E International* **103** (2019), 154–165.

[2] S. Marelli and B. Sudret, "UQLab: a framework for uncertainty quantification in Matlab", *Vulnerability, Uncertainty, and Risk*, 2554–2563.

[3] J. Kennedy and R. Eberhart, "Particle swarm optimization", *Proceedings of ICNN'95 - International Conference on Neural Networks*, vol. 4, 1995, 1942–1948.

[4] B. Sudret and C. Mai, "Computing derivative-based global sensitivity measures using polynomial chaos expansions", *Reliability Engineering & System Safety* **134** (2015), 241–250.

[5] M. Noel, "A new gradient based particle swarm optimization algorithm for accurate computation of global minimum", *Appl. Soft Comput.* **12** (2012), 353–359.

[6] S. Ahmed et al., "Real-time flaw characterization through learning-by-examples techniques: a comparative study applied to ECT", *Electromagnetic Nondestructive Evaluation (XX)* **42** (2017), 228–235.

[7] S. Bilicz, "Sensitivity analysis of inverse problems in EM non-destructive testing", English, *IET Science, Measurement & Technology* **14** (5 2020), 543–551(8).

A Micro EIT Sensor for Real-Time and Label Free Biological Imaging

Antonio AFFANNI[a], Ruben SPECOGNA[a,1], Francesco TREVISAN[a]
and Antonello TAMBURRINO[b,c]
[a] *Polytechnic Dept. of Engineering and Architecture, University of Udine, Udine, Italy*
[b] *Dipartimento di Ingegneria Elettrica e dell'Informazione 'M. Scarano', Università degli Studi di Cassino e del Lazio Meridionale, Cassino (FR), Italy*
[c] *Department of Electrical and Computer Engineering, Michigan State University, East Lansing, MI 48824, USA*

Abstract. A micro electrical impedance tomography (EIT) sensor with radially distributed planar electrodes was designed, characterized, and experimentally validated for the real-time and label free imaging of insulators inside a physiological solution. The reconstruction algorithm used is based on a Monotonicity Principle and it is appealing because it is noniterative and real-time.

Keywords. Electrical impedance tomography, monotonicity principles, monotonicity reconstruction algorithm, 3d cell culture, label-free imaging, real time imaging

1. Introduction

The problem addressed in this contribution is the fast imaging of insulating objects inside a conducting fluid. A typical application in this context is the imaging of 3d cell cultures that grow in a physiological solution. Optical imaging methods are costly, bulky and do not work with opaque fluids unless some fluorescent label is applied.

Starting from 1980's [1], Electrical Impedance Tomography (EIT) is one of the electrical tomographic imaging modalities to visualize non-intrusively the electrical conductivity within a region of interest (ROI) [1]. Methods based on electric fields are appealing because they are label-free, faster and cheaper with respect to optical alternatives. The principle of EIT is to apply successively an electrical current on various sets of electrodes and measure the induced voltages on the other electrode pairs. With these information, a map of the conductivity is obtained with an algorithm that solves the inverse problem.

This paper proposes a micro electrical impedance tomography (EIT) sensor [2] designed to be miniaturized and realized with inexpensive fabrication methods. First of all, the sensor is characterized by radially distributed *planar* electrodes, in such a way that it can be realized in printed circuit board (PCB) technology to monitor cell cultures growing in a well or by patterning the microelectrodes on an insulating substrate to be used inside lab-on-a-chip devices. The well is filled by a physiological solution and the ROI is identified in the interior of the electrodes, see Fig. 1.

[1], E-mail: ruben.specogna@uniud.it.

The second peculiarity of the sensor it that the measurement electronics and protocol are designed to be used with a noniterative and real time imaging technique based on a monotonicity property [3]. This imaging method can treat insulators with arbitrary shapes, topologies and even multiple insulators.

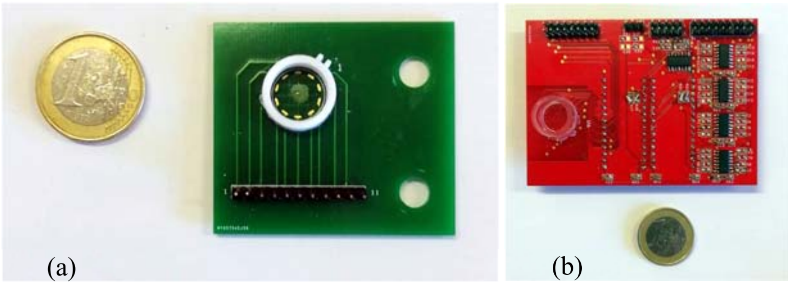

Figure 1. (a) Gold plated electrodes realized in PCB technology and the well.
(b) The signal conditioning board.

The reconstruction method requires a special measurement protocol, because there is the need to obtain all the entries of a resistance matrix Ř [3]. In particular, given the resistance matrix R_D relative to a known test domain D placed in the fluid, it is possible to assess whether the test domain D is contained in the insulator by checking if Ř- R_D is positive semi-definite. Covering the ROI with many test domains allows the reconstruction of the shape of the insulator. It is advantageous that the test defects are partially overlapping each other to obtain a better representation of the insulator's shape.

Another difference with respect to the literature is that usually the resistance matrices of the set of defects are obtained by a numerical simulation. In our case, the resistance matrices are obtained experimentally by means of automated measurements via an accurate positioning system.

An example of the reconstructed defect is represented in Fig. 2.

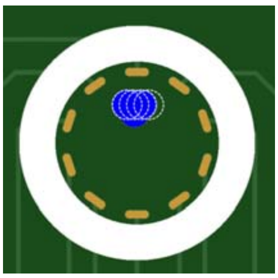

Figure 1. An example of a reconstruction obtained with the proposed method. The union of the dashed test domains form the real shape of the insulator. The union of the blue test domains for the reconstructed shape.

References

[1] D. C. Barber and B. H. Brown, Applied potential tomography, *J. Phys. E Sci. Instrum.* **17** (1984), 723-733.

[2] A. Affanni, R. Specogna, A. Tamburrino, and F. Trevisan, Imaging of insulating media in a physiological solution by means of Electrical Impedance Tomography (2022).

[3] A. Tamburrino, G. Rubinacci, "A new non-iterative inversion method for Electrical Resistance Tomography", *Inverse Problems* **18** (2002), 1809-1829.

Wireless RF Multifrequency Resonator for the Non-invasive Monitoring of Tumors in Breast Tissues

Alexiane PASQUIER [a,1], Yohan LE DIRAISON [b], Stéphane SERFATY [b] and Pierre-Yves JOUBERT [a]

[a] *C2N, CNRS, Université Paris-Saclay*
[b] *SATIE, CNRS, Cergy Paris Université*

Keywords. non-contact sensor, multifrequency RF resonator, dielectric characterization

Early detection of breast cancer is one of the major issues for women health. To prevent and monitor such disease, several techniques have been developed such as MRI, mammography, or echography. Besides, for incident electromagnetic waves in the radio frequency (RF) bandwidth (tens to hundreds of MHz), several teams discovered that a high dielectric contrast, around 70 %, regarding both the electrical conductivity σ and the relative permittivity ε_r, exists between malignant and non-malignant breast tissues [1]. Those dielectric parameters are frequency dependent, and highly relevant to detect early physiophathological changes in tissues in a possibly non-invasive way [2]. In [3], an inductive high-Q resonator, based on a passive transmission line resonator (TLR) used as a transmit-and-receive antenna, has been used to monitor a tissue burn, confirming the interest of such non-contact sensor to monitor tissues alterations. The aim of this paper is to propose the use of a novel inductive wireless multifrequency resonator (WMFR), combining several TLR, to detect and localize dielectric changes in tissues.

The WMFR used in this study, denoted WMFR-4, is constituted of four TLR arranged in a nested configuration as shown Fig. 1. It consists of four circular double-sided conductive tracks, each having opposite gaps on both sides of a dielectric substrate, constituting TLR 4 to TLR 1. These TLR have diameters of 2, 3.5, 5.5 and 8.5 cm and track width of 1, 2.5, 5, 10 cm, respectively. They feature resonance frequency of 250, 98, 47 and 21 MHz respectively, and quality factors above 250. Each of them is modelled with an electrically equivalent $R_n L_n C_n$ circuit with $n \in [1,4]$ (Fig. 1). The WMFR-4 is managed by inductive coupling to a distant single loop RF probe connected to a vector network analyzer. The probe equivalent electrical circuit $R_s L_s$ is shown in Fig. 1. The influence of the tissue placed in the vicinity of the WMFR-4 sensor is modeled by inductance L_{i_n} and resistance R_{i_n} with n$\in [1,4]$, standing for the relative permittivity and the conductivity of the tissue, respectively [3]. From the electrical circuit of Fig. 1, the impedance of the RF probe Z_{mes} in a narrow bandwidth centered around the resonance frequency of TLR n is expressed by:

[1]This work was supported by LabeX LaSIPS (ANR-10-LABX-0040-LaSIPS) managed by the French National Research Agency (no.ANR-11-IDEX-0003-02)

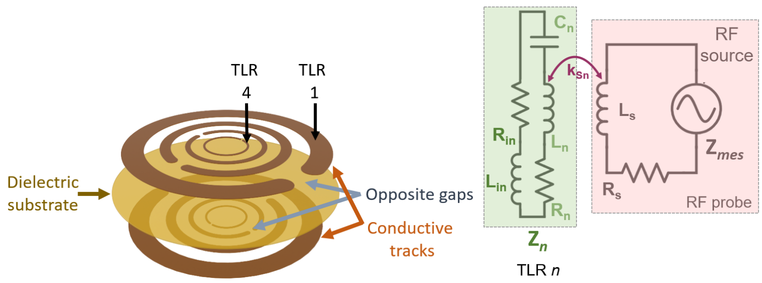

Figure 1. Left : exploded view of the used WMFR-4; Right : equivalent electrical circuit of each constitutive TLR.

$$Z_{\text{mes}} - Z_{\text{S}} = \frac{C_n k_{\text{S}n}^2 L_{\text{S}} L_n j(2\pi f)^3}{1 + C_n(R_n + R_{\text{i}_n}) j2\pi f + C_n(L_n + L_{\text{i}_n})(j2\pi f)^2} \tag{1}$$

where $Z_{\text{s}} = R_{\text{s}} + j\omega L_{\text{s}}$ and $k_{\text{S}n}$ is the coupling coefficient between the RF probe and TLR n. In this equation only $R_{\text{i}_n} L_{\text{i}_n}$ are unknown, the other parameters being previously analytically or experimentally estimated. The experimental setup is presented Fig. 2. The RF probe is placed at 0.5 cm of the WMFR-4 which is placed next to a deionized water recipient ($\sigma \approx 0$ and $\varepsilon_{\text{r}} \approx 80$), and a PTU95A hollow sphere of 1.5 cm diameter filled with a saline solution ($\sigma = 5.7$ S/m and $\varepsilon_{\text{r}} \approx 80$) is moved inside the water recipient thanks to a robotic arm, in a scanning plane perpendicular to the WMFR-4. For each position of the sphere, the measurement of Z_{mes} is adjusted against the complex model of Eq. (1), so that an estimate of R_{i_n} and L_{i_n} is carried out at the four frequencies. The resulting complex modulus $|Z_{\text{i}}| = |R_{\text{i}_n} + j\omega L_{\text{i}_n}|$ is plotted versus the position of the sphere in Fig. 2.

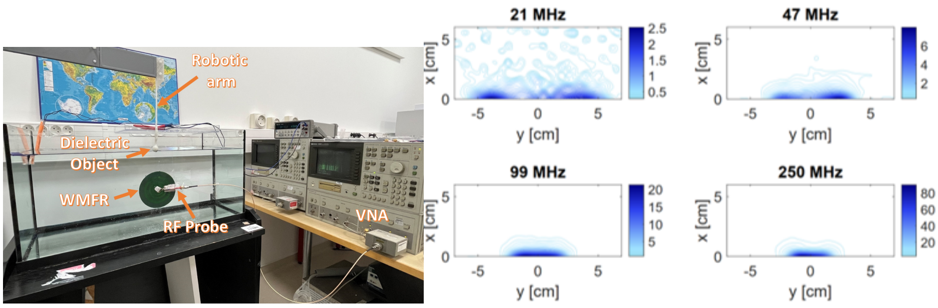

Figure 2. Left : experimental setup; Right : estimated impedance modulus $|Z_{\text{i}_n}|$ for the 4 resonance frequencies of the WMFR-4 at each position of the dielectric object.

The obtained results demonstrate the ability of the WMFR-4 to sense the presence of the dielectric sphere in four different regions defined by the geometries of the involved TLR, and at four different frequencies. This kind of sensor opens the way to the development of a new generation of sensors sensitive to dielectric properties modifications of tissues, with frequency and space selectivity.

References

[1] W. T. Joines, Y. Zhang, C. Li, and R. L. Jirtle, “The measured electrical properties of normal and malignant human tissues from 50 to 900 Mhz,” *Medical Physics*, vol. 21, no. 4, 1994.

[2] C. Gabriel, “Dielectric Properties of Biological Materials,” 2006.

[3] T. H. N. Dinh, S. Serfaty, and P. Y. Joubert, “Non-contact radiofrequency inductive sensor for the dielectric characterization of burn depth in organic tissues,” *Sensors (Switzerland)*, vol. 19, no. 5, 2019.

Data fusion and non-destructive testing of damaged fiber-reinforced laminates

Valentin NOËL [a,b], Thomas RODET [a], and Dominique LESSELIER [b,1]

[a] *Systèmes et Applications des Technologies de l'Information et de l'Energie, Ecole Normale Supérieure Paris-Saclay, Gif-sur-Yvette, France*

[b] *Laboratoire des Signaux et Systèmes, Université Paris-Saclay, CNRS, CentraleSupélec,Gif-sur-Yvette, France*

Abstract. Efficient strategies for non-destructive testing of damaged composite laminates modeled from homogenization of fiber-reinforced polymers could involve fused data. Here, those are from electromagnetic and infrared thermographic modalities, for which semi-analytical models of the interaction are available. Focus is on inter-layer delaminations. Paths forward are outlined, mostly within the realm of Bayesian approaches and of convolutional neural networks, both of wide breadth and the second ones not involving too many prior regularization factors.

Keywords. Electromagnetics, thermography, composites, data fusion

Composite materials are widely used in automotive industry, aeronautics, and green engineering, since low cost, light weight, and of large strength/ and stiffness/weight ratios vs. traditional materials. Yet their non-destructive testing may be highly challenging, with need for more modeling and computational imaging, before envisaging sound laboratory-controlled experimentations.

Active thermography as a contactless procedure is more and more used for inspection of isotropic work pieces, refer to [1] and references therein, but an increasing volume of contributions appears on fibered laminates, with strong emphasis on carbon-fiber-based ones —those exhibiting strong anisotropic behavior due to their thermal conductivity function of orientation, e.g., [2]— as illustrated in the recent review [3], with deep learning coming also to the fore [4]. In rather sharp contrast, electromagnetic probing of such composite structures appears much less studied, possibly since standard eddy-current probes tend not to work so well for carbon-fiber-based laminates, and may call for tailor-made sensors [5] in the MHz range and beyond, so as usual eddy-current hypotheses fail.

The above stated, focused on thermographic and electromagnetic modalities of inspection, one needs (i) proper mathematical and physical models of damaged laminates, (ii) versatile enough codes that can provide a good amount of accurately simulated data when those assumed to be inspected by both modalities, and last but not least, (iii) computational imaging tools that can fuse in a proper way the information which those data provide independenty, with the benefit of absence of registration since the structure is unchanged during testing. The three-fold challenge is strong and simplifications are needed.

[1] Corresponding Author: dominique.lesselier@centralesupelec.fr.

The first simplification is that intact laminates are homogeneous per horizontal ply and exhibit within each ply an uniaxial anisotropic behavior, which is manifested by a transverse and longitudinal dielectric permittivity or thermal conductivity, being underlined that one has the joint benefit that first-order electromagnetic homogenization [6] holds close to the same in thermography.

The second simplification is that damages generally can be seen as thin flat delaminations occuring between plies, which is not too demanding for the electromagnetic Green-dyadic-based semi-analytical approaches in [7], while they are amenable in thermography (in the case of a flash lamp as heat source at least) to extension of the Truncated Region Eigenfunction Expansion (TREE), so far applied to isotropic laminates [1], since only the heat equation is impacted by the uniaxial behavior.

The third simplification is that one has available imaging tools that can cope with data provided by the two modalities. So, if data simulated on a host of damages, double-stream convolutional neural networks (CNN) appear the way forward, also having insurance that brute force codes (FEM) could always provide good data, if the semi-analytical algorithms were to fail in some cases. This approach was shown highly effective in [8] for fused ultrasound and microwave imaging, if enough physics within it to guide to sound solutions, with the additional advantage that a stand-alone solution with a single modality can always be developed. With now the advantage of far less data needed than with CNN, the Bayesian framework as also devised for breast imaging in [9] enables in principle to bypass the need of many priors on regularisation factors (those are produced in effect during the construction of the maps of the damages) while there should be good profit in the Bayesian formalism to draw from the assumption of thin delaminations.

To conclude, this preliminary investigation aims at pointing out that data fusion should enable testing of carbon-fibered-based laminates. Semi-analytical solutions are indeed capable at least in simple enough cases (thin inter-layer delaminations) to yield proper data to mimick electromagnetic and thermographic inspections, once the intact structures properly homogenized. Then, data from both modalities could be fused, e.g., in deep learning and Bayesian realms, as inspired, e.g., from [8,9].

References

[1] A. Ratsakou *et al.*, Shape reconstruction of delamination defects using thermographic infrared signals based on an enhanced Canny approach, *Infrared Phys. Technol.* **111** (2020), 103527.

[2] S. Bard *et al.*, Influence of fiber volume content on thermal conductivity in transverse and fiber direction of carbon fiber-reinforced epoxy laminates, *Materials* **12** (2019), 1084.

[3] F. Ciampa *et al.*, Recent advances in active infrared thermography for non-destructive testing of aerospace components, *Sensors* **18** (2018), 609.

[4] Z. Tong *et al.*, Automated defect detection in CFRP using flash infrared thermography and deep learning method, *2nd European NDT & CM Days*, Prague, *NDTnet* **2021-12** (2021), 10 pp.

[5] H. Heuer *et al.*, Review on quality assurance along the CFRP value chain – Nondestructive testing of fabrics, preforms and CFRP by HF radio wave techniques, *Composites Part B*, **77** (2015), 494–501.

[6] C. Li and D. Lesselier, On homogenization of fiber-reinforced polymers, *Radio Scie. Lett.* (2022), to appear, 5 pp.

[7] Y. Zhong *et al.*, Fast calculation of scattering by 3-D inhomogeneities in uniaxial anisotropic multilayers, *IEEE Trans. Antennas Propagat.*, **62** (2014), 6365-6374.

[8] Y. Qin *et al.*, Breast imaging by convolutional neural networks from joint microwave and ultrasonic data, *IEEE Trans. Antennas Propagat.* (2022), Early Access, 12 pp.

[9] Y. Qin *et al.*, Fused microwave and ultrasonic breast imaging within the framework of a joint variational Bayesian approximation (2022), submitted.

Tomography of Nonlinear Magnetic Materials via the Monotonicity Principle

Antonio CORBO ESPOSITO [a], Luisa FAELLA [a], Vincenzo MOTTOLA [a], Gianpaolo PISCITELLI [b], Ravi PRAKASH [c] and Antonello TAMBURRINO [a,d]

[a] *Dipartimento di Ingegneria Elettrica e dell'Informazione "M. Scarano", Università degli Studi di Cassino e del Lazio Meridionale, 03043, Cassino, Italy.*

[b] *Dipartimento di Matematica e Applicazioni "R. Caccioppoli", Università degli Studi di Napoli Federico II, 81026, Napoli, Italy.*

[c] *Departamento de Matemática, Universidad de Concepción, Concepción, Chile.*

[d] *Department of Electrical and Computer Engineering, Michigan State University, East Lansing, MI-48824, USA.*

Abstract. Here we treat the inverse problem of the reconstruction of the nonlinear magnetic permeability, starting from boundary measurements in the static limit. In this framework, the Monotonicity Principle (a monotonic relation connecting the unknown material property to the measured data) is at the foundation for a class of non-iterative and real-time imaging methods [1].

Differently from the linear and p-Laplacian cases [2], the Monotonicity Principle (MP) for the DtN (Dirichlet-to-Neumann) operator does not hold. Therefore, we introduce a new boundary operator, the Average DtN operator, for which a MP hold [3]. Finally, we provide some numerical evidence of the monotonicity for the nonlinear case.

1. The Nonlinear Permeability Problem

In this work, we present a theoretical contribution to the field of inverse problems with nonlinear constitutive relationships. From a general perspective, it is worth noting that the mathematical analysis for inverse problems governed by nonlinear Maxwell's equations is still in the early stages of development.

The target problem is to reconstruct the shape of region Q, contained into the domain of interest Ω, consisting of a non linear magnetic permeability, immersed in a uniform background characterized by a linear permeability.

Let Ω be simply connected and let ψ be the scalar potential, which gives the magnetic field as $\mathbf{H}(x) = -\nabla\psi(x)$. Assuming the constitutive relationship to be $\mathbf{B}(x) = -\mu\,(x, \|\psi\|)\,\mathbf{H}(x)$, the magnetostatic problem can be formulated as:

$$\begin{cases} \nabla\cdot(\mu(x,\|\nabla\psi\|)\nabla\psi(x)) = 0 & \text{in } \Omega \\ \psi(x) = f(x) & \text{on } \partial\Omega. \end{cases} \tag{1}$$

μ depends on H only in the unknown region Q. The problem is globally non linear. The Monotonicity Principle holds for the Average DtN operator $\overline{\Lambda}_\mu$, in the sense that [3]:

$$\mu_1 \leqslant \mu_2 \Longrightarrow \langle \overline{\Lambda}_{\mu_1}(f), f \rangle \leqslant \langle \overline{\Lambda}_{\mu_2}(f), f \rangle \; \forall f \tag{2}$$

where μ_1 and μ_2 are the permeabilities, $\overline{\Lambda}_\mu$ is the Average DtN operator defined as $\overline{\Lambda}_\mu(f) = \int_0^1 \Lambda_\mu(\alpha f)\, d\alpha$ and Λ_μ is the DtN operator. Let us stress that $\mu_1 \leqslant \mu_2$ means $\mu_1(x,H) \leqslant \mu_2(x,H)$ for a.e. $x \in \overline{\Omega}$ and $\forall H \geq 0$.

2. Numerical example

In this section we test numerically the monotonicity condition in (2). We consider a non linear magnetic material placed in a uniform background made of a linear material. The non linear material is electrical steel M330-50A, with magnetic permeability μ_{NL}. The linear material is ferrite, with magnetic permeability $\mu_L = 1000\mu_0$, which is strictly smaller than μ_{NL}, for any H. Hereafter we denote with μ_A a magnetic permeability equal to μ_{NL} in A and equal to μ_L in $\Omega \setminus A$. The domain Ω is a $10\,mm \times 10\,mm$ square. We consider three test configurations: Q, $T_1 \subset Q$ and $T_2 \nsubseteq Q$, as represented in Figure 1. Then, we apply some different boundary data f and we compare $\mathbb{F}_A = \langle \overline{\Lambda}_{\mu_A}(f), f \rangle$, for A equals to Q, T_1 and T_2 (see Table below). As expected, $\mu_{T_1} \leqslant \mu_Q$ implies $\mathbb{F}_{T_1}$ always less or equal to $\mathbb{F}_Q$. Instead, since $\mu_{T_2} \nleqslant \mu_Q$, there exists a boundary data such that $\mathbb{F}_{T_2} > \mathbb{F}_Q$.

f	$\mathbb{F}_Q - \mathbb{F}_{T_1}$	$\mathbb{F}_Q - \mathbb{F}_{T_2}$
$200x$	0.3483	0.3028
$10x^2 + 10x^3$	0.4238	-0.2018
$50x^2 + 50\sin(y^2)$	0.2326	-0.1160

We conclude by remarking that this is the first numerical evidence of the Monotonicity Principle for non linear materials.

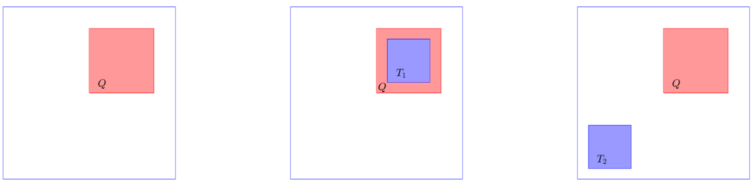

Figure 1. Domains Q (left), T_1 (center) and T_2 (right). They are square boxes of side $3.75\,mm$, $2.5\,mm$ and $2.5\,mm$, respectively. The nonlinear material is placed in the coloured boxes.

References

[1] A. Tamburrino, G. Rubinacci, A new non-iterative inversion method for electrical resistance tomography, *Inverse Problems* (2002).

[2] M. Salo, X. Zhong, An inverse problem for the p-laplacian: Boundary determination, *SIAM Journal on Mathematical Analysis* (2012).

[3] A. Corbo Esposito, L. Faella, G. Piscitelli, R. Prakash, A. Tamburrino, Monotonicity Principle for Tomography of Nonlinear Conducting Materials, *Inverse Problems* (2021).

Monotonicity based Imaging Method using Time-Domain Eddy Current Measurements

Zhiyi SU[a,1], Lalita UDPA[b], Gianpaolo PISCITELLI[c] and Antonello TAMBURRINO[b,d]
[a] *Zhejiang Lab, Hangzhou, Zhejiang 311121, China*
[b]*Department of Electrical and Computer Engineering, Michigan State University, East Lansing, MI 48824, USA*
[c]*Dipartimento di Matematica e Applicazioni "R. Caccioppoli", Università degli Studi di Napoli Federico II, 81026 Napoli, Italy*
[d]*Department of Electrical and Information Engineering, Università di Cassino e del Lazio Meridionale, 03043, Cassino, Italy*

Abstract. Monotonicity Principle (MP) provides the foundation for fast and non-iterative imaging methods. Specifically, MP of time constants and MP of transfer functions have been proposed for eddy current imaging. In this contribution, we propose a complete imaging algorithm based on Monotonicity Principle of transfer functions, using time-domain eddy current measurements. Numerical examples related to the imaging of the shape of cracks in conductive materials are also presented. The numerical examples have been carried out in a realistic setting, including the modelling of the noise.

Keywords. Inverse Problems, Imaging, Eddy Current Testing, Monotonicity based Methods.

1. Introduction

Imaging problems in nondestructive testing and evaluation attempts to precisely determine the existence, location, size and shape of an unknow defect. Monotonicity Principle Method (MPM) is a fast and non-iterative imaging approach that was first introduced in [1] for electrical resistance tomography. MP of time constants was later discovered to process time-domain eddy current measurements [2] and was then extended to non-linear materials [3]. This contribution focuses on the problem of eddy current tomography via MPM of transfer functions [4] to estimate the defect shape. This specific modality is still at the early stage of development [4], and overcomes some limitations related to MPM of time constants [2].

2. Imaging Method and Validation

The eddy current problem considered in this work consists of a conductive specimen and an array of coil sensors. The transfer function ***Z*** is defined as follows:

[1] E-mail: dantesuu@gmail.com.

$$v_{mn}(t) = Z_{mn}(\tau) i_n(t) + O(e^{-t/\tau_1}), \text{ for } t \to +\infty \text{ and } i_n(t) = I_n e^{-t/\tau} \quad (1)$$

where $v_{mn}(t)$ is the pick-up coil voltage due to the eddy currents and measured at the m-th coil when the n-th coil is driven by the current $i_n(t) = I_n e^{-t/\tau}$, where I_n is a constant and $\tau > \tau_1$ is prescribed. The monotonicity of the transfer function is stated as $A_1 \subseteq A_2 \Rightarrow \boldsymbol{Z}_1(\tau) \leq \boldsymbol{Z}_2(\tau)$, where A_1 and A_2 are two insulating anomalies in a conducting media.

Noise is assumed to be additive w.r.t. measured coil voltages, i.e. $\tilde{v}_{nm}(t) = v_{nm}(t) + d(t)$, where $d(t)$ is a Gaussian distributed random variable with zero mean and standard deviation of δ, where $\delta = \epsilon \max_{n,m,t} |v_{nm}(t)|$.

The numerical example refers to the inspection of an aluminum plate (6mm x 6mm x 3mm). Two eddy current coil arrays are arranged above and below the aluminum plate, respectively. A zero-thickness defects is assumed in vertical (symmetry) plan of the two sensor arrays. Figure 2 shows the true defect profile and the reconstruction under different noise levels using the imaging method described in Eq. (2). More numerical results will be presented and discussed in the full paper. The location, size and shape of the defect can be retrieved with noise level up to $\epsilon = 10^{-4}$. At higher noise levels, a degradation of spatial resolution is experienced.

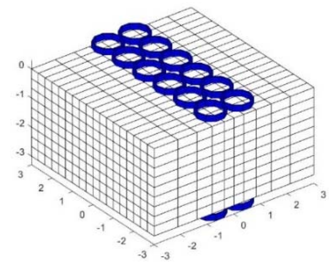

Figure 1. Two arrays made by 12 coils are placed on the top and bottom of the sample. Each coil has an inner diameter of 0.9 mm, an outer diameter of 1 mm, a height of 0.2 mm and a liftoff of 0.1 mm.

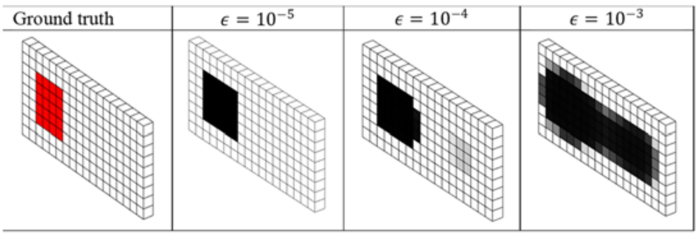

Figure 2. Ground truth and reconstructions of a defect at different noise levels.

References

[1] A. Tamburrino and G. Rubinacci, A new non-iterative inversion method for electrical resistance tomography, *Inverse Problems* **18**.6 (2002), 1809.

[2] Z. Su, S. Ventre, L. Udpa, and A. Tamburrino, Monotonicity based imaging method for time-domain eddy current problems, *Inverse Problems* **33**.12 (2017), 125007.

[3] A.C. Esposito, L. Faella, G. Piscitelli, R. Prakash, A. Tamburrino, Monotonicity Principle in tomography of nonlinear conducting materials, *Inverse Problems* **37**.4 (2021), 045012.

[4] Z. Su, Monotonicity based imaging methods for pulsed eddy current testing, PhD Thesis, 2018

Efficient design of remote field eddy current array probe for imaging of defects in small diameter ferromagnetic tube

T. Vijayachandrika, S. Thirunavukkarasu, Anish Kumar
Nondestructive Evaluation Division,Indira Gandhi Centre for Atomic Research
A CI of Homi Bhabha National Institute, Kalpakkam, Tamil Nadu-603102, India
Email: vijayachandrika@igcar.gov.in

Abstract

This paper reports the design optimisation of a radial segmented coil based remote field eddy current(RFEC) array probe for imaging of defects in small diameter steam generator tube made of modified 9Cr-1Mo ferritic steel. Systematic experimental and model-based studies were carried out to optimise the spatial pitch, number of coils, and coil size of the array probe. Studies revealed that an 8-element receiver coil probe is optimum for detection and imaging of flaws with a signal to noise ratio greater than 10 dB.

Keyword: Imaging, array probe design, remote field eddy current, finite element modelling

1 Introduction

Imaging in electromagnetic non-destructive evaluation (NDE) has grown tremendously in the recent past towards achieving improved detection and sizing of defects in the tubular components.Attempts have been made in remote field eddy current (RFEC) technique for imaging defects by way of designing segmented coil to detect and image defects in large diameter pipes and tubes [1]. Recent studies have also shown that a segmented radial coil probe is promising for imaging of defects in small diameter tubes [2]. However, design and development of an array probe with is a challenging especially for smaller diameter tubes such as the one used for the steam generator of fast breeder reactors.This paper discusses the results of experiemental studies to optimize the number of coils, diameter, height and spacial pitch between the coils for full circumferential coverage with supported 3D finite element model. Finite element modeling using COMSOL software has been carried out to support the experimental results findings.

2Result and discussion

A single element radial receiver coil has been fabricated and mounted on an Z-θ scanner capable of linearly moving the probe inside the tube and rotating the tube at specified angles for imaging of defects. The experimental parameters of the probe and reference defects considerd in the studies are given in Table 1. A through hole of 1.2 mm diameter is considered, asper the ASME standard used during the quality control of the tubes.

Table 1: Parameters of the RFEC probe used in simulation and experiment studies

S.no	Type	Probe parameter	Material and defect details
1	Experiment	Receiver exciter distance: 37mm Exciter turns: 200 (34 SWG), Receiver Turns: 200 (40 SWG)	Defect: Through holes of diameter 5 mm, 2.3 mm, and 1.2 mm

2.1 Experimental Results

A modified 9 Cr-1 Mo steam generator tube with a 1.2 mm through holes was inspected using the single element RFEC receiver coil probe. The probe was scanned in the ID side of the tube at a constant speed of 1mm/sec. The amplitude observed for1.2 mm, 2.3 mm and 5 mm holes holes were measured at different angular positions of the probe with respect tothe holes (0 degree) as shown in Fig 2a. It can be seen that the amplitude is highest when the probe is exactly below the defect (at 0 degree) and decreases on either side in a Gaussian fashion. The amplitude falls to a defect free value at approximatey 20 degrees on either side. In order to accurately find out the probe response in the circumferential direction, the full width at half maximum (FWHM) of the amplitude distribution has been computed by fitting it to a Gaussian function.The FWHM has been foundto be 43.7° for the 1.2 mm hole. A radial segemented coil of 4 mm diameter and 4 mm height has also been found to be optimial after systematic experimental trials by varying the coil size. Considering the coil size, the extent of its response (~45°) and the tube inner diameter (12.2 mm), 8 number of radial type receiver coil probe was found to be optimum for reliably detecting defects. Imaging of the through holes was made with the 8 coil probe with 2 layers of four coils staggered axially. Figure 2b shows that the probe could successfully image the 1.2 mm hole with an SNR greater than 10 dB.3D finite element modeling studies were also carried out to confirm the findings and the same will be presented in the paper.

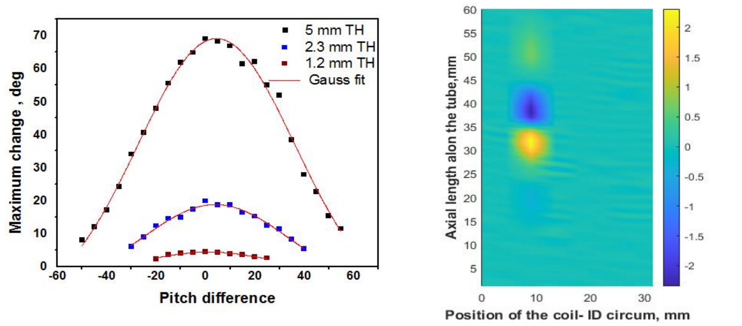

Figure 2: (a)Measured amplitude variations of 5 mm, 2.3 mm and 1.2 mm diameter through holes (THs) along the circumferential direction and b) RFEC base corrected phase image of 1.2 mm diameter hole.

3Conclusion

A Systematic experimental and FE modeling studies have been carried out to optimise the design of a radial type RFEC array probe. A prototype probe with 8 number of radial type array receiver coils staggered in two rows (with four coils each) has been developed and used to image 1.2 mm through hole in modified 9Cr-1Mo steam generator tube. The SNR has been found to be more than 10 dB.

References

[1]. T. Vijayachandrika, S. Thirunavukkarasu, B, Purnachandra Rao, “Comprehensive study on radial coil influence in designing segmented remote field eddy current probe for defect detection in ferromagnetic tubes”, Nondestructive Testing and Evaluation (2021) (T&F),(online).

[2]. B. Purna Chandra Rao, Baldev Raj, T. Jayakumar, P. Kalyanasundaram. “An intelligent imaging scheme for automated eddy current testing”,Nondestructive Testing and Evaluation (T&F),17(2001), 41-57.

Small Diameter Array Probe with TMR Sensors and Elliptical Excitation for Thimble Tube Inspection

Jingyi Wang[a], Xinchen Tao[a] and Chaofeng Ye[a,b]
[a] *School of Information Science and Technology, ShanghaiTech University, Shanghai, China.*
[b] *Shanghai Engineering Research Center of Energy Efficient and Custom AI IC*

Abstract. Thimble tubes in a nuclear power plant are used to insert detectors to measure the distribution of neutron fluence rate of the nuclear reactor core, core power distortion, and accumulating burnup data. It is important to inspect the thimble tubes' damage timely to avoid accidents and economic losses. However, it is challenging to develop a small array probe that suits thimble tubes whose diameter is only 5mm. This paper presents a new probe with array tunnel magnetoresistance (TMR) sensors and elliptical excitation coil for thimble tube inspection. The probe consists of 8 TMR sensors, which are wire bonded on a circuit board together with a bare die operational amplifier chip. A magnetic field image is generated by the probe in a scan, which is sensitive to both circumferential and axial defects due to the elliptical excitation. A prototype probe has been developed and tested.

Keywords. array probe, eddy current testing, TMR sensor, nuclear inspection, elliptical excitation

1. Introduction

The thimble tube is an important part in a nuclear power plant. Typically, bobbin probes are employed for thimble tube inspection, which can only generate line data[1]. Array probe can output an inspection image in a scan. However, it is challenging to develop such a small array probe that satisfies diameter limitation of 5mm. Most eddy current testing (ECT) array probes use induction coils to pick up signals, which faces a physical limitation of the coil sizes. TMR sensors have enhanced spatial resolution, high sensitivity in wide frequency bandwidth and small mutual inductance compared with coils [2].

2. Probe Design and Experiment Result

This paper presents a small diameter probe with array TMR sensors for thimble tubes inspection. The structure of the probe is as shown in Figure 1(a). The probe contains 8 TMR sensors, which are wire bonded on an elliptical printed circuit board (PCB) whose major and minor axes are 5mm and 9mm, as shown in Figure 1 (b). The sensors' sensing directions are perpendicular to the edge of the PCB. In addition, a bare die 8 to 1 multiplexer chip is also wired bonded on the PCB. An operational amplifier and circuit connectors are soldered on the back of the PCB. The PCB is placed inside a 3D printed plastic skeleton, which maintains the liftoff distance almost constant during the inspection. An elliptical coil is wounded outside of the sensor array as the excitation coil. The excitation coil has 35 turns of wires. The inner major and minor axes, outer major and minor axes and height of the elliptic coil are 8.6mm, 4.3mm, 9.48mm, 4.74mm and 1mm respectively. To effectively detect axial and circumferential defects, the sensor array and excitation coil are placed obliquely related to the axis of the tube, that is, the excitation current direction and the axial of the probe form an angle α (α=30°).

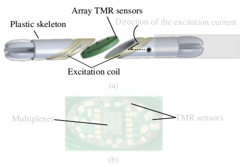

Figure 1 (a) diagram of the probe design (b) picture of the printed circuit board with the TMR array sensors and bare die multiplexer

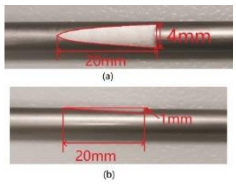

Figure 2 Photograph of the thimble tube with an artificial defect: (a) front view and (b) side view

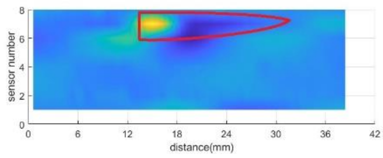

Figure 3 Experiment image of quadrature component of the probe outputs of the artificial defect

The feasibility of the proposed probe is validated experimentally by testing a thimble tube sample with an artificial defect. The material of the sample is stainless steel. The inner and outer diameter of the tube sample are 5 mm and 8.65 mm respectively. The shape and dimensions of the defect are as shown in Figure 2. The excitation coil is driving by a sinusoid voltage source, the amplitude and frequency of which are 5V and 30kHz respectively. The outputs of the TMR sensors are multiplexed and digitalized by a multiplexer ADG408. The excitation voltage is digitalized simultaneously as a reference signal. Then the in-phase and quadrature component of the signals of the TMR sensors are calculated. The quadrature component image of the defect is depicted in Figure 3. It is seen that the defect can de clearly identified from the image. The image shape is correlated with the size of the defect meaning that it may be possible to quantify the defect from the image.

3. Conclusion

This paper presented a small diameter array array probe for thimble tube inspection. Primary experiment results showed that the probe can image defect on the thimble tube sample. It is possible to calculate the sizes of the defect from the output image. In the future, the probe will be tested extensively, when more defects will be inspected and the images will be analyzed.

References

[1] L. ZHANG *et al.*, “Swept-frequency ET and innovative feature extraction of abrasion defects for thimble tubes in nuclear power plants,” *China Mechanical Engineering*, vol. 32, no. 01, p. 18, 2021.

[2] N. Zhang, C. Ye, L. Peng, and Y. Tao, “Eddy Current Probe with Three-Phase Excitation and Integrated Array TMR Sensors,” *IEEE Transactions on Industrial Electronics*, pp. 1–1, 2020.

Eddy current sensor interface from frequency output sensors to LDC based integrative eddy current test

Guiyun Tian[1,2] , Xiaolong lu[3]

[1.]School of Engineering, Newcastle University, NE1 7RU, UK;

[2.] School of Automation Engineering, University of Electronic Science and Technology of China, Chengdu 611731, China

[3.]School of Mechanical Engineering, Sichuan University, Chengdu 610065, China

Abstract

Sensors' signal conditioning and digital interface are important for sensor technologies, digital transformation and the Internet of Things (IoTs) in particular. Frequency output sensors and inductance-to-digital converter (LDC) have demonstrated significant advantages in comparison with conventional sensors with Analog-to-Digital Converter (ADC) interfaces. This paper reviews eddy current signal conditioning and digital interface in the field of displacement sensors and non-destructive test & evaluation (NDT & E). After review and comparison of different signal conditioning and digital interface, LDC chip is used for multiple parameter measurement including equivalent inductance via frequency measurement and transient responses through pulsed excitation. A novel pulse eddy current non-destructive testing method based on LDC is proposed. This method uses LDC pulse excitation coil to measure the inductance change of the coil, and the envelope line of the ADC capture transient excitation is used to measure the impedance change of the coil. Based on the standard specimen as the test object, the defect depth and frequency relationship experiment, the defect and envelope slop relationship experiment, and lift-off experiment are carried out on the LDC-based pulse eddy current detection method. Experimental results show that this method is feasible, and the research results help to miniaturized pulsed eddy current flaw detection equipment. This work illustrates integrated approach of signal conditioning and digital interface for multiple parameter or feature measurement for integrated eddy current NDT. The work open a new way for addressing multiple parameter measurement of eddy current NDT & E including lift-off estimation and multiple pulsed eddy current via digital interface. It has potential to bridge the gaps of metrology of geometry, displacement measurement and NDT & E for defect detection and material characterisation.

Key words: Digital interface; Frequency output sensors; LDC interface sensors; LDC based pulse eddy current detection; Multiple parameter

1. Introduction

Eddy current testing (ECT) is a non-destructive testing method based on electromagnetic induction, which is suitable for surface or near-surface defect detection of conductive materials and composite materials containing conductive components. ECT has become one of the most widely used NDT technologies for material characterization, defect detection and metal thickness measurements in industrial production. To overcome the shortcomings of single frequency ECT, several excitation methods have been applied to ECT. And, there has been great progression in the study of ECT in lift-off distance, defect detection and material characterization. However, at present, ECT can only measure these parameters separately. Their separation remains a challenge for some critical application areas, such as oil-gas pipeline inspection, where simultaneous measuring lift-off, defect or material characterization is required.

Thus to bridge the gap, LDC chip based hybrid eddy current sensor system developed for displacement or lift-off measurement, defect defection and characterization is presented and evaluated in the paper.

2. Hybrid eddy current sensor systems and studies

Fig.1 (a) illustrates the block diagram of the measurement principle of the proposed hybrid eddy current sensor. It includes LDC1614, LC resonator composed of an inductor (coil) in parallel with a capacitor *C*, and transient signal acquisition circuit. The LDC provides an AC current matching the sensor resonator frequency across the LC resonator. The change in coil inductance can be obtained by measuring the frequency of the LC resonator. And the envelope line of the ADC capture transient excitation is used to measure the impedance change of the coil. The inductance and impedance of the coil are the function of target distance, target material, and sensor characteristics. A typical eddy current probe is used for our proposed hybrid signal condition system as illustrated in Fig. 1(b) with a sample of three man-made slots of same widths and different depths of 0.2, 0.5, 1.0 mm.

(a)

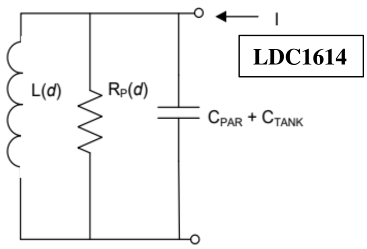

(b)

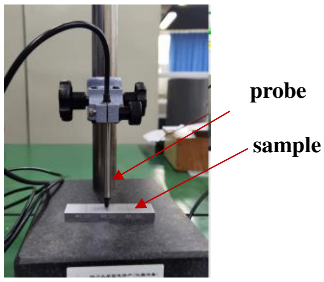

Fig. 1 The measurement principle and experimental setup of hybrid eddy current sensor

3. Initial tests

As illustrated in Fig. 2, different frequency outputs and transient responses are produced monotonically. It can be seen from Fig.2 (a), the frequency of the LC resonant circuit corresponds to the depth of the defects. At the same time, we use transient signal acquisition circuit to obtain the envelope of the transient signal. Fig. 2(b) is the first derivative of the envelope curves of the defect and sound area.

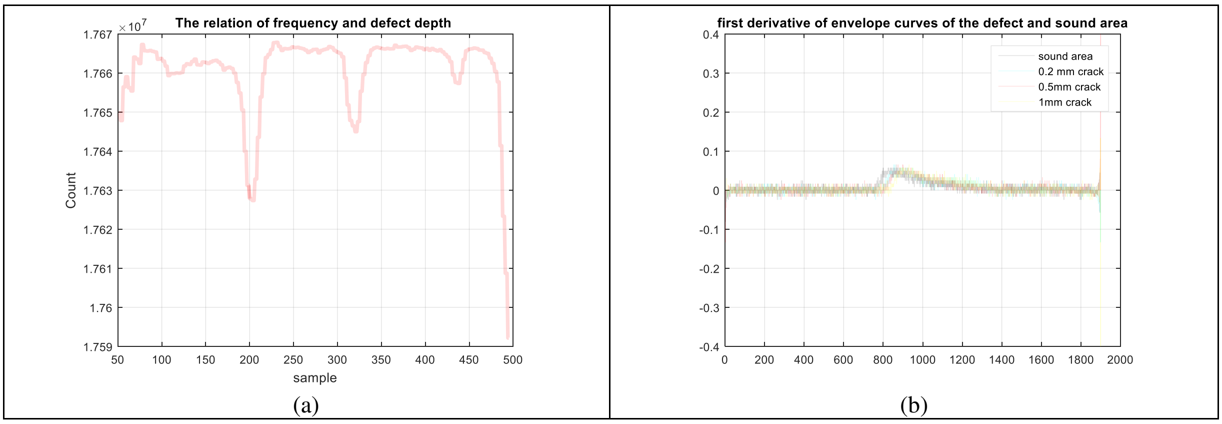

(a) (b)

Fig. 2 Frequency output and transient responses of hybrid signal conditionings for eddy current NDT

4. Conclusion and future work

The conclusions are drawn from this study:

(1) The depth of the defect, the lift-off can be characterized by the frequency count value of the LC resonator.

(2) The transient excitation signal envelope of the LDC output can also characterize the depth of the defect.

Future works include quantitative analysis and instrument miniaturization.

Purpose and Practical Capabilities of the Metal Magnetic Memory Method

Anatoly DUBOV [a,1], Peter LADANYI [b], Sergey KOLOKOLNIKOV [a]
[a] *Energodiagnostika Co. Ltd, Russia*
[b] *Hideg Neutron Forrás Kft Hungary*

Abstract. The main purpose of the metal magnetic memory (MMM) method is determination in the express control mode of stress concentration zones (SCZs) – the main sources of developing damages – on equipment and in structures using specialized instruments and scanning devices. SCZs are not only areas, which are known beforehand, where structural features create various conditions for distribution of stresses created by external load, but these are also randomly located areas where, due to initial metal heterogeneity, large strains occur in combination with off-design additional workloads. Inspection by the MMM method is carried out without metal dressing or artificial magnetization. Residual magnetization, formed naturally in the course of products manufacture and during their operation, is used.

Keywords. Metal magnetic memory, non-destructive testing, stress control, stress-strained state

The metal magnetic memory (MMM) method, which appeared in Russia in the early 90s of the XX century and gained recognition at the level of an international ISO standard [1], [2], is currently being actively developed in Europe, America and Asia.

The fundamentally new magnetic method of non-destructive testing (NDT) is based on the use of residual magnetization that has formed naturally during products manufacture and in the course of their operation under conditions of a weak geomagnetic field. It was proposed by the authors of the MMM method that this magnetization, which experts considered and still continue to consider as interference (noise) in the development of electromagnetic NDT methods, should be used for the purposes of technical diagnostics.

The presented regularities, established between the natural magnetization and the mechanical characteristics of the metal, led to emergence of the metal magnetic memory concept.

The MMM method uniqueness is that it is based on the use of the self-magnetic stray field (SMSF) occurring in stress concentration zones (SCZs) due to metal inhomogeneities and defects formed during products manufacture or under the effect of workloads under the conditions of their operation[3].

The studies found that variation of products magnetization during operation is due to the magnetoelastic and magnetomechanical effects, as well as magnetoplastics. It was also found that variation of the measured self-magnetic leakage field H during tension, compression, torsion and cyclic loading, for example, of ferromagnetic pipes is unambiguously related to the maximum acting working stresses, which allowed to use this parameter as a memory element during the MMM method development [4], [5].

Basic practical advantages of the new diagnostics method as compared to the known magnetic and other traditional methods of non-destructive testing are:

- special magnetizing devices are not required as the phenomenon of equipment and structures units magnetization in the process of their operation is used;
- locations of stress concentration due to working loads, which are unknown beforehand, are determined in the course of their inspection;
- metal dressing or any other preparation of the test surface is not required;
- the MMM method can be applied both at the test object operation and at its repair;
- small-sized instruments with self-contained power supply, recording devices and a memory unit up to 1 Gb are used for inspection by the proposed method;
- special scanning devices allow testing of pipelines, vessels and equipment in the express-control mode at a speed of 1000 m/h and more.

The main task of the MMM method is detecting on the test object of the most dangerous sections and units characterized by stress concentration zones. Then, using, for example, ultrasonic inspection in stress concentration zones, the presence of a specific defect is detected.

Metallurgical and technological manufacturing defects create in local areas of products a high level of residual stresses (RS), which remain undetected due to imperfections of the used NDT methods. For engineering products the MMM method allows to ensure 100% quality control and their sorting in mass production, as well as control of local residual stress zones.

The MMM method is the most suitable practical NDT method at assessment of actual stress-strained state. The method allows performing an integral evaluation of a unit state, taking into account the metal quality, actual operating conditions and its structural features. Therefore application of the new diagnostics method is the most effective for equipment life assessment.

The paper considers examples of the practical application of the MMM method in diagnostics of equipment and structures.

[1] ISO 24497-1:2020 Non-destracteve testing-Metal magnetic memory-, Part1:Vocabulary and general requirements

[2] ISO 24497-1:2020 Non-destractive testing-Metal magnetic memory-, Part2:Inspection of welded joints

[3] A.A.Dubov Metal Magnetic Memory Method. History of Origin and Development.Moscow:FSUE “Izvestiya”Publishing House UD P RF, 2011-256p.

[4] A.A.Dubov,V.T.Vlaszov:Phisical basic of the Matel Magnetic Mamory Moscow,2004,2019. Moszkva

[5] A.A.Dubov,V.T.Vlaszov:Phisical Theory of the “Strain-Failure”process Part I.,PartII.,Moscow,2013

Probability of detection considering both the depth and circumferential length of pipe wall thinning using microwave NDT

Yijun GUO[a,1], Takuma TOMIZAWA[a], Noritaka YUSA[a], Hidetoshi HASHIZUME[a]

[a] *Department of Quantum Science and Energy Engineering, Graduate School of Engineering, Tohoku University, 6-6-01-2, Aramaki Aza Aoba, Aoba, Sendai, Miyagi 980-8579, Japan*

Abstract. This study proposes a method to calculate the probability of detection (POD) using TM_{01} mode microwaves as a function of both the depth and circumferential length of pipe wall thinning. Experiments were conducted to construct a multivariate regression model considering the amplitude of reflection signals, wall thinning depth and circumferential length. A two-dimensional POD model was constructed based on the obtained regression model. The POD contour demonstrates the good detection capability of microwave testing against wall thinning with different depths and circumferential lengths even at a long distance.

Keywords. Two-dimensional POD, TM_{01} microwaves, Multivariate regression

1. Introduction

Microwave NDT is effective in the fast inspection of a long pipe because of its fixed transmit-receive probe. Its basic principle is that the metal pipe works as a waveguide, and microwaves propagating inside it are reflected if there is a defect on the inner surface. To assess the detection performance of microwave NDT, a POD model was built considering the depth and location of full circumferential wall thinning [1]. However, the circumferential length of wall thinning, which is also important, was not considered in the previous POD model. Thus, this study proposed a two-dimensional POD model considering the depth and the circumferential length of wall thinning to assess the detection capacity of microwave NDT. In addition, the sensitivity of reflection signal amplitude to the depth and circumferential length was studied in experiments.

2. Materials and Methods

The experimental setup is illustrated in figure 1. Microwaves of TEM mode at 12.1-21.1 GHz (1.4 MHz step) were converted to TM_{01} mode by a TEM-TM_{01} probe. Generated TM_{01} mode microwaves were used to detect the wall thinning in a 15-m-long straight pipe. A joint with wall thinning structure, characterized by depth d and length l and circumferential length θ, was inserted using a flange connection into the main pipe to emulate the wall thinning at the location of 13.5 m. Emulated d and θ ranged 0.2-2.0 mm and 45°-360°, respectively. The average amplitude of processed reflection signal $\hat{y}$ for 3 measurements using each joint was used for the following multivariate regression.

From simulation results, which will be presented in the conference, the influence of l on $\hat{y}$ is negligible relative to that of d and θ. In addition to linear relationships among

[1] Yijun GUO, Corresponding author, Department of Quantum Science and Energy Engineering, Graduate School of Engineering, Tohoku University, Sendai, Miyagi, Japan; E-mail: guo.yijun.r1@dc.tohoku.ac.jp.

logarithmic values of these parameters, which is illustrated in section 3, we can obtain:

$$\ln(\hat{y}) = C_1 \times \ln(d) + C_2 \times \ln(\theta) + C_3 + \varepsilon \tag{1}$$

where C_1, C_2, and C_3 are the undetermined coefficients and will be determined by multivariate regression; $\varepsilon \sim N(0, \sigma)$ is a random error term, postulated to be normally distributed with the mean of 0 and the standard deviation of the residual of the multivariate regression. Then, POD is calculated by:

$$\mathrm{POD} = \Phi\left(\frac{C_1 \times \ln(d) + C_2 \times \ln(\theta) + C_3 - \hat{y}_{th}}{\sigma}\right) \tag{2}$$

where Φ denotes the cumulative distribution function of the standard normal distribution and $\hat{y}_{th}$ is the decision threshold, determined by measured noise.

3. Results and discussions

Figure 2 presents the linear relationship among $ln(\hat{y})$, $ln(d)$ and $ln(\theta)$, which confirms the feasibility of Eq. (1). Parameters in Eq. (1) and (2) were determined by multivariate regression using experimental results: C_1=0.8719, C_2=1.0440, C_3=-8.9537, σ=0.1232. The value of C_1 and C_2 implies that the reflection amplitude is more sensitive to θ than d. This is also verified by the influence of d-θ combinations at the same volume of wall thinning on reflected signals as shown in figure 3. Calculated POD contour in figure 4 indicates wall thinning with d=0.019 mm and θ=360°can be reliably detected with the lower 95% confidence bound of 0.9 POD, which will be verified in future.

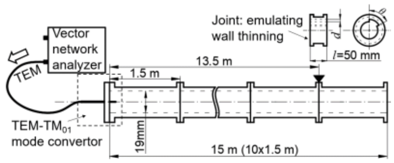

Figure 1. Experimental setup.

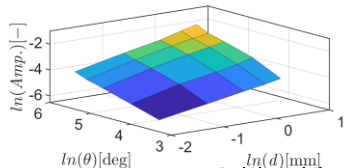

Figure 2. Relationship among $ln(\hat{y})$, $ln(d)$ and $ln(\theta)$.

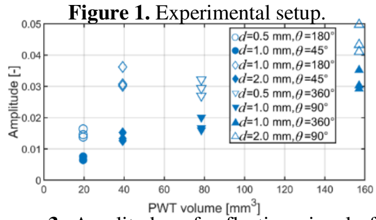

Figure 3. Amplitudes of reflection signals from wall thinning with the same volume but different dimensions.

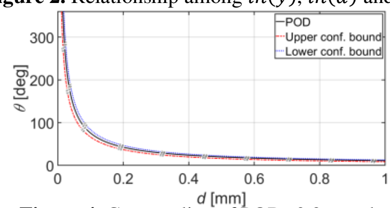

Figure 4. Contour line of POD=0.9 together with the 95% confidence bounds.

4. Conclusions

This study proposed a multivariate POD model considering wall thinning depth and circumferential length and proved the good detection capacity of microwave NDT to detect wall thinning at a long distance of 13.5 m, according to POD analysis. In addition, a larger influence of circumferential length on the amplitude of reflection signals indicates the importance to consider circumferential length in the POD analysis.

References

[1] G. Chen, Y. Guo, T. Katagiri, et al. Multivariate probability of detection (POD) analysis considering the defect location for long-range, non-destructive pipe inspection using electromagnetic guided wave testing. *NDT & E International*, **124** (2021), 102539.

Hardware and Software Design for a Battery-powered Portable Pulsed Eddy Current (PEC) System

Lei Xiong[a], Zihan Xia[a], Ruochen Huang[a], Jialong Shen[b,c] and Wuliang Yin[a,1]

[a] *Department of Electrical and Electronic Engineering, University of Manchester, Manchester, M13 9PL, UK*

[b] *Key Laboratory of New Processing Technology for Nonferrous Metal & Materials, Ministry of Education/ Guangxi, Guilin University of Technology, Guilin 541004, China.*

[c] *Collaborative Innovation Center for Exploration of Nonferrous Metal Deposits and Efficient Utilization of Resources, Guilin University of Technology, Guilin 541004, China*

Abstract. The design of a battery-powered pulsed eddy current (PEC) portable system is in urgent need for the evaluation of corrosion in oil, gas and power generation industry. An ARM Cortex microcontroller is applied to generate excitation signal, measure magnetic field via a tunnel magnetoresistance (TMR) sensor, and control measurement channels and the process. The hardware has been integrated into an instrument with the size of 21mm×18mm×18mm. In terms of software, the graphical user interface (GUI) is based on Qt5 and implemented with the instrument. The GUI features a touchable interaction function provides the magnetic field measurements for various testing configurations. When operating with an extremely low frequency of 1Hz, the system can detect aluminum thickness of 80mm with the ADC sampling rate of 6000 Hz. With a battery life of more than 8 hours, the portable system can fulfil the demands of the industry.

Keywords. Pulsed eddy current, Electromagnetic, Battery-powered instrument

1. Introduction

Pulsed Eddy Current (PEC) has been deployed for the purpose of corrosion-related applications for some time and it is still intensively studied and developed by researchers around the world. This technology can provide an efficient screening tool that can detect corrosion without having to remove coating or insulating material over the samples [1]. Basically, a PEC system consists of an excitation coil, magnetic sensors, conditioning electronics, and microcontroller (MCU) system. The magnetic sensor can convert the magnetic field to the voltage signal for system to measure the variation of the magnetic field due to metallic objectives. The excitation square wave contains an infinite train of sinusoidal waveforms, which can reflect the feature of test sample at a one-time test [2].

The proposed system applied a TMR sensor to provide accurate magnetic field data [3], and an ARM microcontroller embedded with ADCs to decrease the power consumption and circuit scale, which achieves the advanced battery-powered system.

2. System Design

This section presents the hardware and software design of the proposed system. The system shown in Figure 1 includes the instrument with an eddy-current sensor.

---

[1] Wuliang Yin, Corresponding author, Department of Electrical and Electronic Engineering, University of Manchester, Manchester, M13 9PL, UK; E-mail: wuliang.yin@manchester.ac.uk.

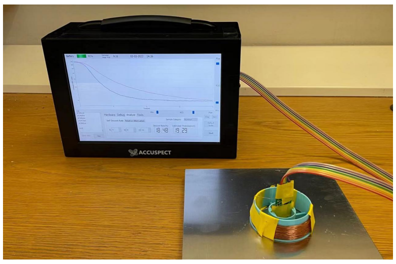

Figure 1. System overview

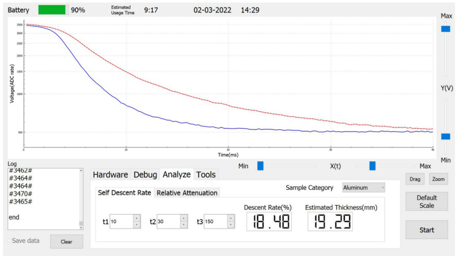

Figure 2. GUI of system

The hardware consists of the front-end driver circuits, communication circuits and MCU minimum system circuit, which are integrated in a portable device with the size of 21×18×18 mm. Front-end driver circuits are for amplification and multiplexing. Communication circuits convert serial port to USB protocol and encode data from MCU to guarantee data integrity. The MCU generates pulsed excitation signal with PWM, reads magnetic field data from the embedded ADC.

For the software, the GUI is developed with Qt5, as shown in Figure 2. The software supports real-time data visualisation, benchmark comparison and thickness estimation, which is ideal for various field measurement applications.

3. Results

The system has been implemented for the measurement of metallic plates, of which the evaluation results are shown in Figure 3. Furthermore, both forward and inverse solvers have been developed and numerical studies carried out for the modelling and simultaneous retrieval of various properties of the object under investigation.

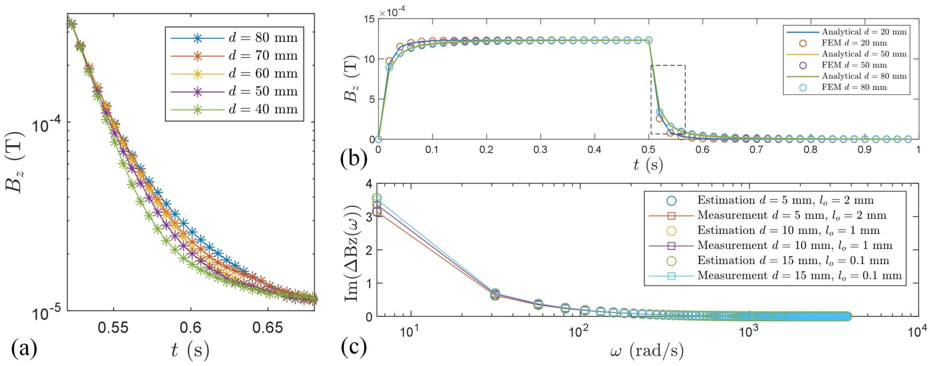

Figure 3. PEC testing results, (a) experimental measurements for aluminium plates of various thickness, (b) forward model results by analytical and FEM solver and (c) the frequency spectra of DP600 plate obtained from simulation and inverse solution.

References

[1] A. Sophian, G. Tian, and M. Fan, "Pulsed Eddy Current Non-destructive Testing and Evaluation: A Review," *Chinese Journal of Mechanical Engineering,* vol. 30, no. 3, pp. 500-514, 2017, doi: 10.1007/s10033-017-0122-4.

[2] Y. He, B. Gao, A. Sophian, and R. Yang, *Transient electromagnetic-thermal nondestructive testing: pulsed eddy current and transient eddy current thermography*. Butterworth-Heinemann, 2017.

[3] A. Ribeiro, H. Ramos, and O. Postolache, "A simple forward direct problem solver for eddy current non-destructive inspection of aluminum plates using uniform field probes," *Measurement,* vol. 45, 02/01 2012, doi: 10.1016/j.measurement.2011.03.029.

Scattering Matrix-based Dielectric Permittivity Estimation of Bulk Materials

Botond Tamás CSATHÓ [a,1], Csaba Endre BERKY and Bálint Péter HORVÁTH [a]

[a] *Department of Broadband Infocommunications and Electromagnetic Theory, Faculty of Electrical Engineering and Informatics, Budapest University of Technology and Economics, Műegyetem rkp. 3., H-1111 Budapest, Hungary.*

Keywords. dielectric permittivity, free-space method, scattering matrix

1. Introduction

Dielectric permittivity estimation of materials is a well-known problem with established theoretical background and measurement practices . In particular free-space methods are capable to determine dielectric properties of materials of various geometries without making direct contact with the specimen [1]. However, most of these methods have their limitations when e.g. the sample thickness, or permittivity exceeds a certain value. However, in some practical cases the material can not be shaped or sliced to arbitrary thickness and geometry, instead a piece of bulk material is present. The most common free-space methods are performed using antennas at one or several frequencies [2]. The estimations are based on a reflection and a transmission measurement characterized by the scattering parameters S_{11} and S_{21}, respectively. Often calibration measurements are also performed without the specimen and/or replacing the specimen with a conductive sheet.

2. Proposed method

In our work we investigate the benefits of using more than two antennas which are placed around the material. Thus, there are not only the two scattering parameters (or 2×2 scattering matrix), but an $N \times N$ scattering matrix is available when using N antennas. In cases when the bulk material is long enough in one dimension the problem can be treated in two dimensions. Thus, we conduct 2D simulations assuming an infinite length in one dimension. We then show what the relationship between the elements of scattering matrix are in function of the dielectric permittivity of the material.

[1] Corresponding Author: E-mail : csatho.botond@edu.bme.hu

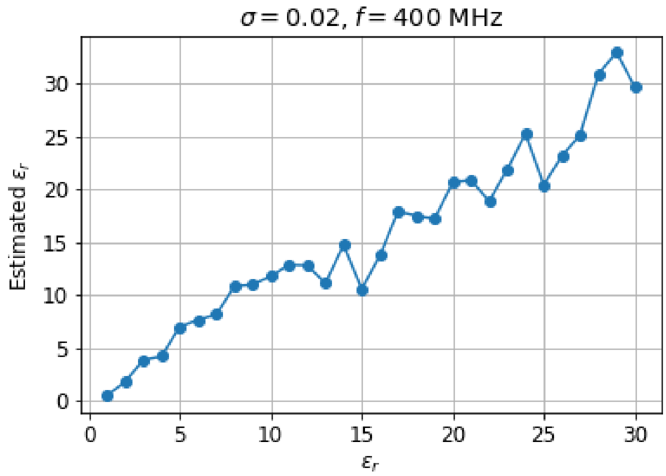

Figure 1. Estimated ε_r using multiple linear regression

3. Results

We performed a simulation where the bulk material is 2×1 meter, and the distance of the antennas is 6 meters and the excitation is a plane wave. The received power at each antenna is estimated by integrating the real part of the Poynting vector on a line element. We then perform a multiple linear regression, where the target variable is the real part of the permittivity ε_r' and the conductivity is constant $\sigma = 0.02$ for a single frequency. In figure 3 we show the result of the linear regression. It can be seen that even for a bulk material the estimated permittivity is within an acceptable range.

References

[1] J. Krupka, "Frequency domain complex permittivity measurements at microwave frequencies," *Measurement Science and Technology*, vol. 17, no. 6, pp. R55–R70, apr 2006.

[2] F. Gonçalves, A. Pinto, R. Mesquita, E. Silva, and A. Brancaccio, "Free-space materials characterization by reflection and transmission measurements using frequency-by-frequency and multi-frequency algorithms," *Electronics*, vol. 7, no. 10, p. 260, oct 2018.

Identification of constitutive parameters of ferrite cores in common mode chokes

Bálint PINTÉR, Arnold BINGLER [1], József PÁVÓ

Budapest University of Technology and Economics, Faculty of Electrical Engineering and Informatics, Department of Broadband Infocommunications and Electromagnetic Theory, Hungary

Abstract. For the accurate 3D modeling of a common mode choke, it is essential to know the frequency dependent permeability of the core. To establish the electromagnetic properties of the core of the choke, a simple impedance analyzer and a partly disassembled CMC is enough. The impedance measured this way is suitable to express the permeability, that can be subsequently used to build an accurate coupled 3D-circuit model of the CMC. This model can be utilized to examine near-field couplings between the choke and other nearby placed filter components, e.g., capacitors.

Keywords. EMI filter, common mode choke, complex permeability, 3D modeling

1. Introduction

In the power supply of electrical devices electromagnetic interference (EMI) filters are widely used to provide noiseless, disturbance free power flow. In the filter, the components are placed close to each other, thereby near-field couplings are present between them, that affects negatively the efficiency of the filter [1]. In order to describe the proper operation of the filter, its circuit model – which is generally used during the design process – should be supplemented with the near-field couplings described by mutual inductances. The latter can be extracted from 3D simulations, provided precise 3D models of the components are at hand [2]. The case of the CMC is especially difficult, apart from handling the frequency-dependent complex permeability of the core, its 3D modeling poses further challenges.

2. Modeling problems

The most significant difficulty of the 3D modeling of the CMC was caused by the coils. In reality the two coils around the toroidal core are irregular, the loops are dense and overlap each other. Instead of building up an even more accurate geometry, it is more advantageous to apply regular coils, with equidistant loops, and compensate with parallel

[1]Corresponding Author: Arnold Bingler; E-mail: arnold.bingler@edu.bme.hu

capacitors to correct the values of the coils' winding capacitances. Another difficult point was obtaining the frequency-dependent permeability and permittivity curves of the core.

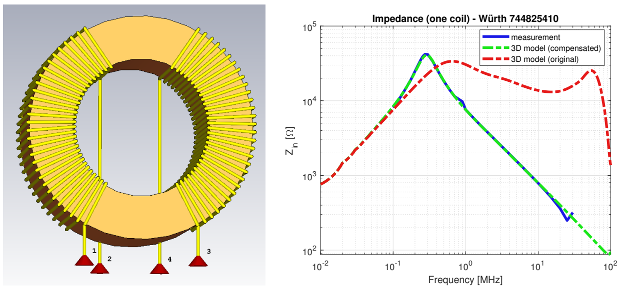

Figure 1. 3D model of the common mode choke (left) and comparison of the measured, simulated and the compensated impedance of the CMC in the one coil case (right)

3. Material parameter identification

The scientific literature offers methods to measure the permeability of a toroidal ferrite core [3], however these are difficult and require expensive instruments (e.g. VNA), or valid only in very high frequencies (GHz range with e.g., waveguide measurements) which is out of the scope of this work. In this method, only an impedance analyzer was used, which is a simple and cheap device, and available for every engineer. The characterization is based on measurements, where the decomposed CMC – consisting of only one coil or one turn – was measured in open-circuit measurement setup. The measured impedance still contains the effects of the coils' winding capacitance and the leakage inductance [4]. However, with some appropriate corrections one can compensate their effects and extract the permeability values from the input impedance as

$$Z_{in} = j\omega\mu^* L, \quad \mu^* = \mu' - j\mu'' = \frac{2\pi Z_{in}}{j\omega\mu_0 N^2 h \ln\left(\frac{R_{out}}{R_{in}}\right)}.$$

With the yielded material parameters and the extra capacitors, an accurate 3D-circuit model of the CMC can be created as depicted in Fig. 1.

References

[1] P. González-Vizuete, F. Fico, A. Fernández-Prieto, M. J. Freire, J. Bernal, "Calculation of Parasitic Self- and Mutual-Inductances of Thin-Film Capacitors for Power Line Filters," *IEEE Transactions on Power Electronics*, vol. 34, no. 1, pp. 236 - 246, 2019

[2] N. Moonen, R. Vogt-Ardatjew, A. Roc'h, F. Leferink, "3-D Full-Wave High Frequency Common Mode Choke Modeling",*IEEE Transactions on Electromagnetic Compatibility*, vol. 62, no. 3, pp. 707 - 714, 2019

[3] C. Domínguez-Palacios, J. Bernal, "Characterization of Common Mode Chokes at High Frequencies With Simple Measurements," *IEEE Transactions on Power Electronics*, vol. 33, no. 5, pp. 3975 - 3987, 2018

[4] C. Cuellar, W. Tan, X. Margueron, A. Benabou, N. Idir, "Measurement Method of the Complex Magnetic Permeability of Ferrites in High Frequency," *IEEE International Instrumentation and Measurement Technology Conference Proceedings*, 2012

Quality control of thermal and thermochemical treatment on mechanical components by electromagnetic methods

H. PETITPRE[a,1], F. ZHANG[a], N. SAMET[b], E.B. NDIAYE[b]

S. BONNIN[c], S. CHOMER[d], C. GALLAIS[e], and L. GAUTIER[f]

[a] *Cetim, 52 avenue Félix Louat 60300 Senlis, France*

[b] *Cetim Grand Est, 21, rue de Chemnitz, 68068 Mulhouse, France*

[c] *Poclain Hydraulics Industrie, Route de Compiègne 60410 Verberie, France*

[d] *Thermi Lyon Développement, 195 Rue de Gerland 69007 - Lyon, France*

[e] *Safran Transmission Systems, 18 Boulevard Louis SEGUIN 92707 Colombes, France*

[f] *Timken Europe, Rue Timken 68002 Colmar, France*

Abstract. Examples of electromagnetic quality control of thermal and thermochemical treatment of mechanical components.

Keywords. Barkhausen noise, 3MA, electromagnetic methods, thermal and thermochemical treatment, nitriding, carburizing, retained austenite, NDE

1. Introduction

Heat and thermochemical treatments of materials are an effective means of optimizing their mechanical properties, ensuring both high hardness and good resistance to contact fatigue, particularly on mechanical transmission components. Today, the quality controls of the heat treatments are generally destructive, costly, and polluting, with a long response time. However, the 100% quality approach and the growing demands of customers, increasingly require rapid and reliable checks on all production. Several electromagnetic methods meet these needs, and are well suited to the problems encountered in treatment processes: (i) measurement of the depth treated in the cases of surface and case hardening, (ii) analysis of multilayers in nitriding, (iii) detection of nonconformities in carburizing: retained austenite ratio / decarburization / presence of carbides, (iv) evaluation of residual stresses linked to the method of production of components, etc.

In this article, we will present 3 industrial applications: nitriding, residual stress, and retained austenite ratio, analyzed with the Barkhausen noise (BN) and the 3MA. These methods, only applicable on ferromagnetic materials, require calibration on parts that are of the same geometry, same material and obtained with the same process, but which cover the range of variability of the characteristic to be monitored.

2. Examples of applications of electromagnetic quality control

- Analysis of nitriding multilayers by 3MA

Two batches of cylindrical samples: one of 18 parts with 6 different nitriding layer depths and a second of 14 parts of a given diffusion layer depth, but with varying levels of compound layer compactness, were analyzed. Calibration was made with a few samples and the rest of the parts were used for validation. The accuracy and fidelity of the estimates obtained are respectively around 0,06 and 0,1 mm for the estimation of the diffusion layer depth, 1,8 and 3 mm for the estimated compound layer depth, and 2 and 4% for the estimation of the compactness of the compound layer.

The 3MA device was also tested on real parts with success: injection rings treated with gas nitriding and tooth flanks treated with deep nitriding.

- Evaluation of residual stress by 3MA

A series of case-hardened transmission parts have undergone different mechanical surface treatments to deliberately obtain variable stress profiles on the surface and in depth. By calibrating the 3MA device with surface stresses and subsurface stresses, the 3D image of the stress profile along the entire circumference of the part could be constructed (**Figure 1**).

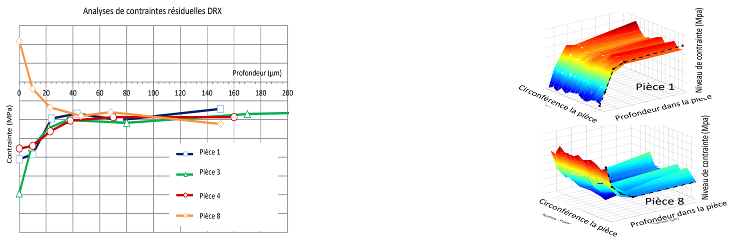

Figure 1. Stress profile of several transmission parts: (Left) X-ray diffraction. (Right) 3MA: top, compressive stress and bottom, tensile stress on surface.

- Retained austenite ratio estimation by 3MA and Barkhausen Noise

A series of 7 batches of 3 carburized bearing rings with different retained austenite ratios were made by varying the tempering conditions (duration and temperature). The retained austenite (AR) ratio was determined with X-ray diffraction. For the 3MA evaluation, the calibration of the testing was performed with 4 parts from different batches, while the rest were for validation. This same series of parts was also analyzed with the BN method. A machine learning analysis was performed on the BN parameters using the Lasso algorithm to define a model of the AR ratio. 2/3 of the parts available were used for the learning process and the last 1/3 for validation of the model. The accuracy and fidelity of the 3MA and BN estimation models of the AR ratio of bearing rings are respectively < 2.5% and 3% with 3MA and 3% and 3% with BN.

3. Conclusion

In this article, we have demonstrated, through some examples, the potential of electromagnetic methods for the quality control of thermal and thermochemical treatments as well as for the characterization of the resulting residual stresses. The main constraint in the implementation of these methods lies in the necessity for calibration of the device used, which can turn out to be complex depending on the application. The more complete the calibration is by integrating all the variability of the production, the more the prediction model will be accurate, and the control will be reliable and robust.

Modelling of carbon fibre composite structures using high-frequency eddy current imaging

Qiuji Yi [a, b] , Paul Wilcox [a] and Robert Hughes [a]
[a] Department of Mechanical Engineering, Ultrasonics and Non-destructive Testing (UNDT), University of Bristol, UK, BS8 1TR
[b] Department of Aerospace Engineering, Bristol Composites Institute (ACCIS), University of Bristol, UK, BS8 1TR

Abstract. High-frequency eddy-current testing (ECT) has previously demonstrated its capability for detecting orientation related features, including fibre orientation and waviness, however, without accurate validated modelling techniques to simulate CFRP features, accurate sensor optimisation and inversion of orientation & material structure cannot be achieved. The lack of suitable models is in part due to CFRP exhibiting highly-complex electromagnetic interactions between fibres, lamina and the ECT sensors, which are difficult to integrate. In this work, a novel finite element modelling approach is proposed to simulate the ECT response to planar multi-layered CFRP components. The fibre tow structure of each unidirectional ply is modelled using orientation dependant 2D conductivity tensor waveforms, and virtual 2D ECT scans are simulated by shifting the waveforms within the model mesh. The results demonstrate that idealised electromagnetic characteristics of the CFRP structure can be successfully modelled compared with experimental data and that 2D ECT data of complex CFRP layers structures can be simulated with improved computational speeds, up to 5x faster compared to standard approaches. The simulation is also used to demonstrate the reduced resistivity losses compared with isotropic materials, caused by the different heterogeneous and multi-layer structures, and predicts high current densities at interfaces of plies with orthogonal orientations, resulting in an effective interface skin-depth.

Keywords. High-frequency eddy current, Carbon fibre reinforced polymer, Fibre orientation, FEM modelling

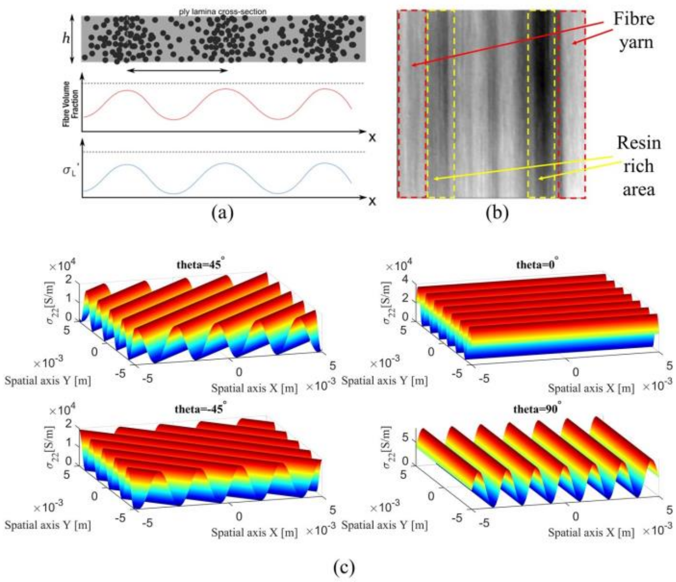

Figure 1 - Demonstration of fibre yarn and resin rich area in experimental ECT data, showing a) the principle proposed for simulated conductivity variation in unidirectional CFRP layer, and b) high-resolution ECT image of unidirectional CFRP, (c) 2D conductivity plane σ_{22} for emulating the CFRP structure

1. Introduction

In previous works, eddy current has been applied for the detection and evaluation of the fibre orientation [1, 2], misorientation (off-axis) as well as in- & out of plane waviness have been characterised by ECT [3, 4].However, the interaction between composite structures and electromagnetic fields remains poorly understood in terms of the current density as a function of depth within CFRP structures and the electrical response of a coil. This hinders the accurate inversion of defects or layer depths based on the fibre orientations[5]. The work in the current paper simulates the electromagnetic modelling of the spatial variation observed in ECT scanning by modelling the electrical conductivity of lamina as a continuous 2D spatial wavefunction to emulate the experimentally observed fibre density variations, as demonstrated in Figure 1(a) and (b). Thus, a multi-layer and spatial variant tensor is calculated to model the composite's electromagnetic properties, shown in Figure 1(c). A virtual ECT scan is simulated over the material using the model to retrieve the electrical properties of the coil, building up a 2D map of coil impedance. The results demonstrate the agreement between modelling and experiments for fibre characterization, as shown in Figure 2, while the limitations of current modelling approaches are discussed.

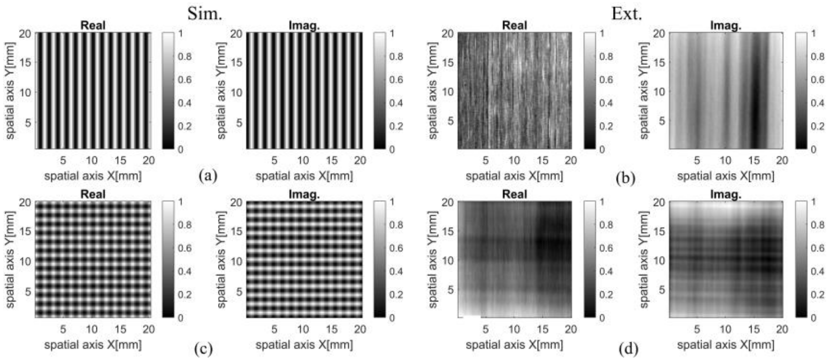

Figure 2 - Comparison of real part and imaginary part of ECT impedance (resistance and reactance) from unidirectional an bi-directional sample. In each row, left two images are simulated data while right ones are experimental ECT data.

References

[1] Cheng J, Qiu J, Ji H, Wang E, Takagi T, Uchimoto T. Application of low frequency ECT method in noncontact detection and visualization of CFRP material. Composites Part B: Engineering. 2017;110:141-52.
[2] Hughes RR, Drinkwater B, Smith R. Characterisation of carbon fibre-reinforced polymer composites through radon-transform analysis of complex eddy-current data. Composites Part B: Engineering. 2018;148:252-9.
[3] Kosukegawa H, Kiso Y, Hashimoto M, Uchimoto T, Takagi T. Evaluation of detectability of differential type probe using directional eddy current for fibre waviness in CFRP. Philosophical Transactions of the Royal Society A. 2020;378:20190587.
[4] Bardl G, Nocke A, Cherif C, Pooch M, Schulze M, Heuer H, et al. Automated detection of yarn orientation in 3D-draped carbon fiber fabrics and preforms from eddy current data. Composites Part B: Engineering. 2016;96:312-24.
[5] Yi Q, Tian G, Malekmohammadi H, Laureti S, Ricci M, Gao S. Inverse reconstruction of fibre orientation in multilayer CFRP using forward FEM and eddy current pulsed thermography. NDT & E International. 2021:102474.

Electromagnetic Methodology for Mechanical Stress Evaluation of Anisotropic Ferromagnetic Materials

Safae BOUTERFAS, Yann LE BIHAN, Laurent SANTANDREA and Laurent DANIEL
Université Paris-Saclay, CentraleSupélec, CNRS, Geeps,
91192 Gif-sur-Yvette, France.
Université Sorbonne, CNRS, Geeps, 75252 Paris, France

Abstract. This work presents an electromagnetic method for mechanical stress evaluation using a U-shaped eddy current (EC) sensor. This technique exploits the magneto-elastic constitutive laws of ferromagnetic materials. Observing the sensor impedance provides information on both the initial magnetic anisotropy and the stress-induced magnetic anisotropy. Measurements from API-5L X52 steel pipelines in the longitudinal (DL) and transverse (DT) directions are used to validate this methodology.

Keywords. Magneto-elastic coupling, Eddy current non-destructive testing, anisotropy, API-5L X52.

1. Introduction

In this paper the EC non-destructive testing using a U-shaped sensor (Fig. 1.a) is employed to detect mechanical stress **T** in anisotropic ferromagnetic material. For a magneto-dynamic problem, the key parameter to include the stress effect is the magnetic permeability μ [1]. μ is sensitive to stress [2], and the electrical conductivity is assumed constant within an applied stress range from 0 MPa to 160 MPa [3]. Therefore, any variation of the measured impedance signal is from magnetic properties once the lift-off is constant.

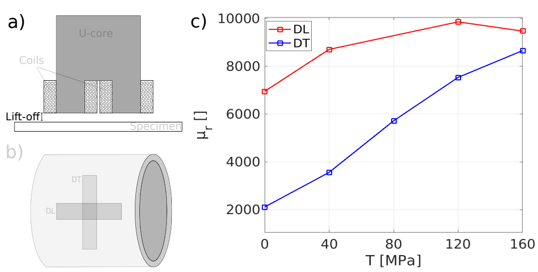

Figure 1. a) Sensor geometry. b) Schematic of specimens cut-out. c) μ_r of DL and DT specimens under stress.

2. Stress effect on the EC sensor impedance

The magneto-elastic characterization of two specimens extracted from an API-5L X52 pipeline[1] in the directions DL and DT Fig. 1.b, shows that the material is anisotropic and that $\mu_r(\mathbf{T})$ increases with respect to uni-axial tensile stresses(Fig. 1.c). Thus the sensor impedance depends on stress. Using a U-shaped EC sensor provides information on the direction of the initial magnetic anisotropy as well as the direction of the induced magnetic anisotropy from uni-axial stresses (Fig. 2). The anisotropy can be estimated by comparing the measured sensor impedance $Z_\theta(\mathbf{T})$ to a reference impedance Z_0 to calculate the relative variation $|\Delta Z_\theta(\mathbf{T})|$, where θ is the angle between the uniaxial stress direction and the sensor orientation, and Z_0 is the impedance for an unstressed material at $\theta = 0$.

3. Results

Z_0 is measured after demagnetizing the specimen. Then a frequency sweep of the impedance is performed for each stress state. Good sensitivity was found for anisotropy detection (Fig. 2.a) and stress evaluation (Fig. 2.b); however, the latter depends on material magnetization M_r. A numerical model of impedance computation will be included in the extended version.

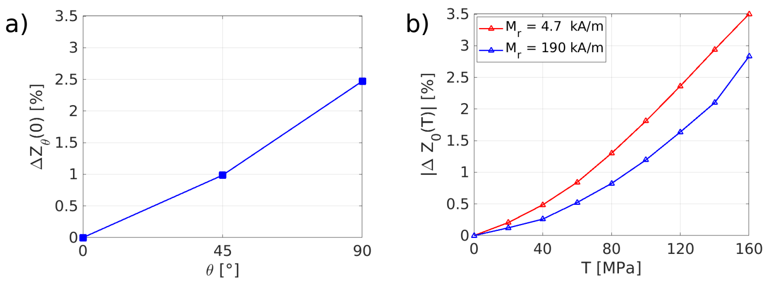

Figure 2. Magnetic anisotropy evaluation at 180 kHz. a) Initial magnetic anisotropy in DL. b) Stress-induced magnetic anisotropy in DL.

References

[1] A. Dahia, E. Berthelot, Y. Le Bihan, and L. Daniel,"A model-based method for the characterisation of stress in magnetic materials using eddy current non-destructive evaluation," *J. Phys. D: Appl. Phys.*, vol. 48, 195002 (2015).

[2] B. D. Cullity, C. D. Graham, Introduction to magnetic materials, 2^{nd}edition, Wiley, New Jersey, 2011.

[3] M. Morozov, G. Yun Tian, and P. J. Withers, "The pulsed eddy current response to applied loading of various aluminium alloys," *NDT & E Int.*, vol. 43, pp. 493–500 (2010).

[1]The specimens were provided by GRTgaz Research & Innovation Center for Energy. Address: 1-3 rue du commandant d'Estienne d'Orves, 92390 Villeneuve La Garenne, France.

Measurement and Modelling Magnetic Anisotropy due to Crystallographic Texture in Interstitial Free (IF) Steels

Mohsen AGHADAVOUDI JOLFAEI [a,1] , Jun LIU [b], Frenk VAN DEN BERG[c], Claire DAVIS[a]
[a] *Warwick Manufacturing Group, University of Warwick, UK*
[b] *School of Engineering, Cardiff University, UK*
[c] *Tata Steel, IJmuiden, Netherlands*

Abstract. Interstitial free (IF) steels are used in the automotive industry for applications requiring good formability, strength and a superior surface quality. The formability is achieved by having a desired strong gamma fibre crystallographic texture, which is typically measured using EBSD or XRD, and is quantified by measuring the r-value from tensile tests. It is desirable to be able to evaluate the crystallographic texture using non-destructive testing on production material. Magnetic anisotropy measurement is an attractive approach as the magnetic behaviour of steel is known to be affected by the crystallographic texture. A set of IF steel specimens, at different states of recrystallisation (commercially cold rolled and annealed to give partially recrystallised and fully recrystallised microstructures) and accordingly different texture components have been used to investigate the measurement and prediction of magnetic anisotropy. A finite element microstructure model that considers crystallographic texture has been developed for the evaluation of magnetic anisotropy in polycrystalline steels. The modelling results have been experimentally validated using a laboratory based electromagnetic (EM) sensor. The results show that the proposed deployable non-destructive approach (U-based sensor that can be placed onto a sheet sample) is promising for the quick evaluation of the magnetic anisotropy in IF steels.

Keywords. Magnetic anisotropy, electromagnetic sensor, crystallographic textures, FE texture model, recrystallisation, Interstitial free steels

Introduction

Interstitial free steels (IF steels) find wide application in the automotive industry, due to their excellent formability. Formability is known to depend on the crystallographic textures present after recrystallisation, and there is a strong correlation between the ratio of near {111} and near {100} texture components; the higher this ratio, the better the formability [1].

Conventionally processed IF steel is hot rolled and coiled, resulting in a randomly textured hot band strip. Cold rolling of this randomly textured material causes the individual crystals to rotate by slip processes towards two sets of orientations, the α fibre set, and the γ fibre set [2]. The strength of these texture components, particularly the α fibre, increases with cold rolling reduction [3]. During the final continuous annealing step the cold rolled steel recrystallises and a strong γ fibre texture develops. It is desirable to be able to measure the extent of texture that develops, for example using magnetic anisotropy, as this can be related to the final product properties and, if measured non-destructively could be used for product quality control during production. There are commercial electromagnetic sensor systems used to non-destructively monitor strip steels during steel production, such as the IMPOC, 3MA and EMspec systems, but these do not currently consider anisotropy and are not used to evaluate texture. There are off-line EM systems used on products or laboratory samples, such as Magnetic Barkhausen Noise (MBN) sensor, Epstein Frame (EPF) and Single Sheet Testers (SST) [4] and these can be used to measure samples machined in different orientations. However, there are no current systems designed to assess crystallographic anisotropy in structural / automotive steels. The aim of this paper lies in investigating the magnetic anisotropy of three IF steel sheets by means of EM sensor measurements and microstructural modelling considering the crystallographic texture.

[1] *Corresponding Author, Corresponding author, Mohsen Jolfaei, mohsen.Jolfaei@warwick.ac.uk.*

Results and discussion

IF steel strips as cold rolled and annealed to different recrystallisation levels have been provided by Tata Steel Europe. Texture analysis was carried out using Electron Back Scattered Diffraction (EBSD). Magnetic anisotropy characterisation was performed using a laboratory EM sensor measuring along different directions with respect to the rolling direction (RD). In this work three IF samples in different heat treatment conditions have been selected: a partially recrystallised IF steel with high density of dislocations (IF-A), a partially recrystallised IF steel with low density of dislocations (IF-B) and a fully recrystallised IF steel (IF-C). In terms of the texture, a mixture of relatively strong α fibre and weak γ fibre in IF-A, a mixture of relatively strong γ fibre and weak α fibre in IF-B and a single strong γ fibre in IF-C (fully recrystallised sample) can be observed, Figure 1 (column left). Kernel Average Misorientation (KAM) values from EBSD characterisation of the samples has been used to evaluate the recrystallisation fraction and correlate that to the texture.

A laboratory based electromagnetic (EM) U shaped sensor, operating at low magnetic field, has been designed to determine the magnetic anisotropy in the IF samples by measuring inductance (which is directly related to the magnetic permeability of the steel) at angles varying from 0° to 90°, in steps of 15°, with respect to the rolling direction. A finite element microstructure model [5] that considers crystallographic texture has been used to predict the magnetic anisotropy in the IF steel samples based on the measured texture, the model potentially can be used in the reverse manner to characterise texture from magnetic measurements. The texture model predicts a strong anisotropic pattern for the fully recrystallised sample which agrees well with that of the measured real inductance value, Figure 1. The predicted and measured values show less agreement for the partially recrystallised samples, this is because the texture model currently does not take into account the effect of the dislocation density present in unrecrystallised grains, which will affect the local magnetic properties (reducing the permeability values). In partially recrystallised samples, where there is a mixture of α-fibre texture grains (typically unrecrystallised with a high dislocation density) and γ-fibre grains (typically recrystallised with a low dislocation density), the model predicted permeability will be higher than the measured permeability and the measured anisotropy will be more affected by the recrystallised grains whereas the model predicts anisotropy from all grains. This will be addressed in future model development.

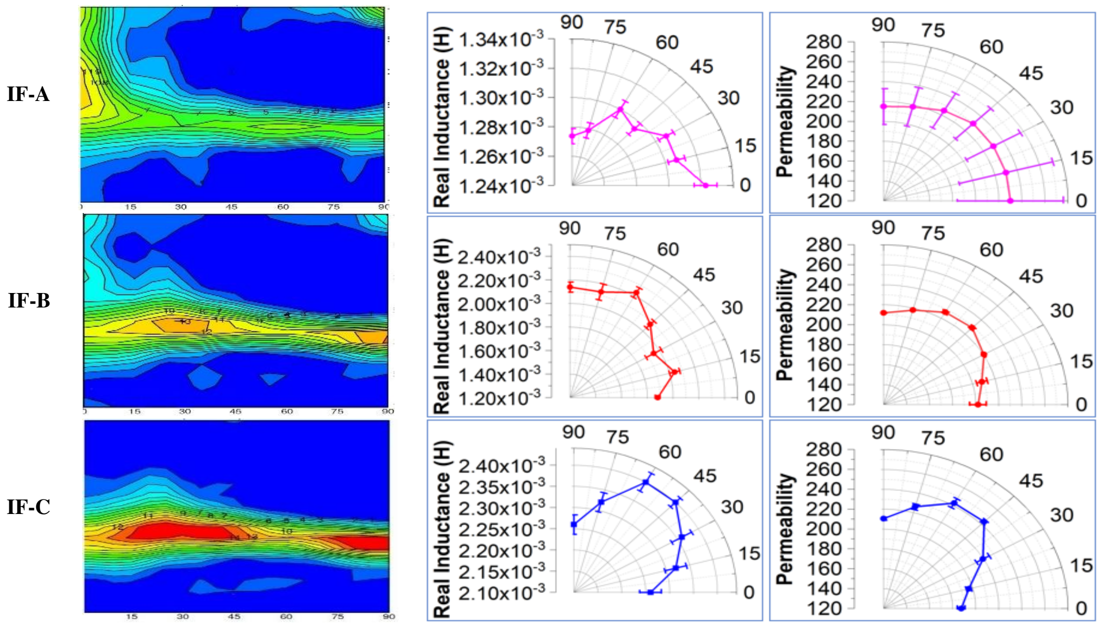

Figure 1. Orientation distribution function (ODF) maps for the three samples studied (left column), real inductance measurements using the EM sensor (middle column) and the predicted magnetic anisotropy using the texture model (right column) for IF-A, IF-B and IF-C.

References

[1]Edmonds, D.V. Designing with Microalloyed and Interstitial-Free Steels. *Handbook of Mechanical Alloy _ Design* **2004**, 321.
[2]Juntunen, P.; Karjalainen, P.; Raabe, D.; Bolle, G.; Kopio, T. Optimizing continuous annealing of interstitial-free steels for improving deep drawability. *Metallurgical and Materials Transactions A* **2001**, *32*, 1989-1995.
[3]Verma, D.; Shekhawat, S.K.; Mukhopadhyay, N.; Sastry, G.; Manna, R. Development of texture in interstitial-free steel processed by equal-channel angular pressing. *Journal of Materials Engineering and Performance* **2016**, *25*, 820-830.
[4]Jolfaei, M.A. Characterisation of Advanced High Strength Strip Steels Using Electromagnetic Sensor System. University of Warwick, University of Warwick, 2019.
[5]Liu, J.; Davis, C. Tensorial permeability microstructure model considering crystallographic texture and grain size for evaluation of magnetic anisotropy in polycrystalline steels. *Philosophical Magazine* **2021**, *101*, 1224-1244.

Effects of Tensile and Comprresive Stress on Magnetic Parameters of Martensitic Stainless Steel

Hiroaki KIKUCHI[a,1] Kohei SUGAI[a] and Keiichi MATSUMURA[b]
[a] *Faculty of Science and Engineering, Iwate University, Morioka, Japan*
[b] *INFITECHM Co., Ltd., Yokohama, Japan*

Abstract. The coercivity changes and Barkhausen noise properties of the martensitic stainless steel with a tensile and compressive stress by a 4-point bending method was evaluated for aiming nondestructive assessment of residual stress of the steel. Both coercivity and Barkhausen noise signal shows monotonically changes against applying stress when the materials have different microstructure states.

Keywords. Corecivity, Barkhausen noise, Stress, quench

1. Introduction

Quantitative assessment of the residual stress on the steel used in turbine components for a thermal power generation plant nondestructively is important. We believe a magnetic method is an effective candidate for such purpose instead of the current X-ray method because magnetic properties are very sensitive to stress and microstructures of the material [1-4]. On turbine components, the steel is quenched to enforce its strength, therefore, the steel has a different microstructure in the same component. Previously, we investigated the effect of quench on magnetic properties and recognized the quench brought to the steel to be hardened in both mechanical and magnetic properties [5].

Here, we also investigate the effect of stress (including compressive and tensile) on the steel with and without quench, which is quite important knowledge for realizing residual stress evaluation using magnetic technique.

2. Experiments and results

Two kinds of martensitic stainless SUS420J steel were used for the experiments. One is base material, and another is quenched sample. The specimen was applied tensile or compressive stress using a 4-poins bending method. The, hysteresis curves and Barkhausen noise signal were measured by a magnetic yoke and a pick-up or an air-core coil, respectively. The hysteresis curves were obtained by integration of induced

[1] Corresponding Author, Hiroaki Kikuchi, Faculty of Science and Engineering, 4-3-5 Ueda, Morioka, Japan; E-mail: hkiku@iwate-u.ac.jp.

voltage at the pickup-coil, and Barkahausen signal was obtained by an amplified and band-pass filtering of voltage at the air-core coil. As to hysteresis curves, coercivity was used for evaluation, and rms voltage was used for Barkhausen noise.

Figure 1 shows the changes in magnetic properties when the specimen was applied stress (here, positive values are tensile stress and negative is compressive). In the figures, "B" means base material, that is, without quench, and "Q" means quench. The coercivity decreases with increasing stress, and absolute value of quench is higher than that of the base. On the other hand, rms values of Barkhausen noise signal increase with increasing stress, and the values of the base are higher than that of quenching. The difference in parameters between base and quench reflects the changes in microstructures. We clarified the quenching decrease grain diameter, which contributes to increased coercivity and to decrease Barkhausen signal [5]. In both cases (base and quenching), magnetic parameter changes monotonically with increasing stress, which is effective to evaluate stress in the material. However, here, we used 4-point bending method for applying stress; this method applied both tensile and compressive stress in the material at the same time. Thus, we need more detail analysis about the obtained results.

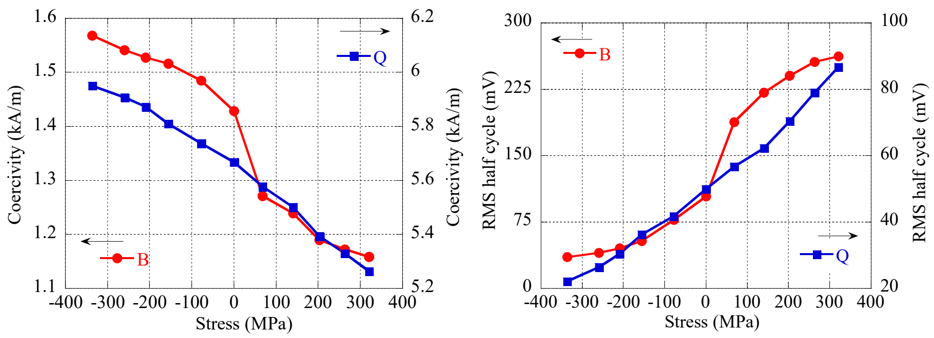

(a) coercivity (b) Barkhausen noise, rms voltage

Figure 1. Stress dependence on magnetic properties of steel without quench (B) and with quench (Q).

References

[1] H. Kronmüller, Magnetic Techniques for the Study of Dislocations in Ferromagnetic Materials, *Int. J. Nondestructive Testing*, **3** (1972) 315–350.

[2] S. Takahashi, J. Echigoya, and Z. Motoki, Magnetization curves of plastically deformed Fe metals and alloys, *Journal of Applied Physics* **87** (2003), 805–813.

[3] C. G. Stefanita, D. L. Atherton and L. Clapham, Plastic versus Elastic Deformation Effects on Magnetic Barkhausen Noise in Steel, *Acta mater*., **48** (2000) 3545–3551.

[4] A. Martínez-de-Guerenu, et al., Nondestructive characterization of recovery and recrystallization in cold rolled low carbon steel by magnetic hysteresis loops, *J. Magn. Magn. Mater*., **316** (2007) e842–e845.

[5] H. Kikuchi, Kohei Sugai, Keiichi Matsumura, Dependence of Corecivity and MBN Signal on Martensitic Stainless Steel with and without Quench, 24th International Workshop on Electromagnetic Nondestructive Evaluation (ENDE2019), Program Book, A0175, 2019.

Mechanical stress estimation through classical and magnetic Barkhausen noise energy hysteresis cycle

Patrick FAGAN, Anastasios SKARLATOS, Christophe REBOUD

CEA, List, Université Paris-Saclay, Palaiseau, F-91129, France.

Laurent DANIEL, Mathieu DOMENJOUD

Université Paris-Saclay, Centrale Supélec, CNRS, Group of electrical Engineering-Paris (GeePs), 91192, Gif-sur-yvette, France.

Benjamin DUCHARNE

ELyTMaX UMI 3757, CNRS – Université de Lyon – Tohoku University, International Joint Unit, Tohoku University, Sendai, Japan.

Abstract. This study establishes relations between applied extern stress and magnetic indicators read on experimental and simulated classic and magnetic Barkhausen noise energy cycles. The objective is to determine the most sensitive magnetic stress indicator and explain why.

1 Introduction

Magnetism can take different aspects in contemporary non-destructive testing [1]. Our group focuses explicitly on the magnetization mechanisms and the evaluation of residual mechanical stresses through these mechanisms.

Mechanical internal stresses are a determinant factor to material performance, structural integrity, and lifetime of industrial systems [2]. Their estimation is of significant interest when anticipating failures and degradations.

Ferromagnetic steels are targeted. They are used in the construction, transportation, and energy domain. The magnetization mechanisms can be classified into five categories [3]:

- the magnetic domain wall bulging (low amplitude range),
- the domain wall irreversible motions (middle amplitude range),
- the magnetization rotation (high amplitude range),
- the domain wall frequency dependence, ripples, and avalanches phenomena,
- the macroscopic eddy currents (skin effect).

These mechanisms exhibit different sensitivity to stress, and a first work consists in establishing these sensitivities. Also, most of these mechanisms are superimposed in a standard magnetization process. Therefore, a second work consists of developing a characterization setup that allows isolation of each mechanism. For this, measurements and simulations can be associated. This study focuses on the mechanical stress influence on standard magnetization B(H) and magnetic Barkhausen noise energy hysteresis MBN_{energy}(H) cycles [4][5].

Experimental results obtained in uniaxial traction situations are confronted with simulation ones to establish the simulation parameters.

A multiscale simulation method based on a statistical distribution of the magnetic domains and the knowledge of the crystallographic texture is used to predict the anhysteretic behavior of both classical and Barkhausen noise cycles [6].

A parametric study of simulation results under tensile stress, and magnetic excitation in every space direction of the lamination plan (FeCo alloy, Fig. 1) allows defining the most stress-sensitive situation. It defines the best magnetic indicator and the best position to observe stress in typical ferromagnetic steels.

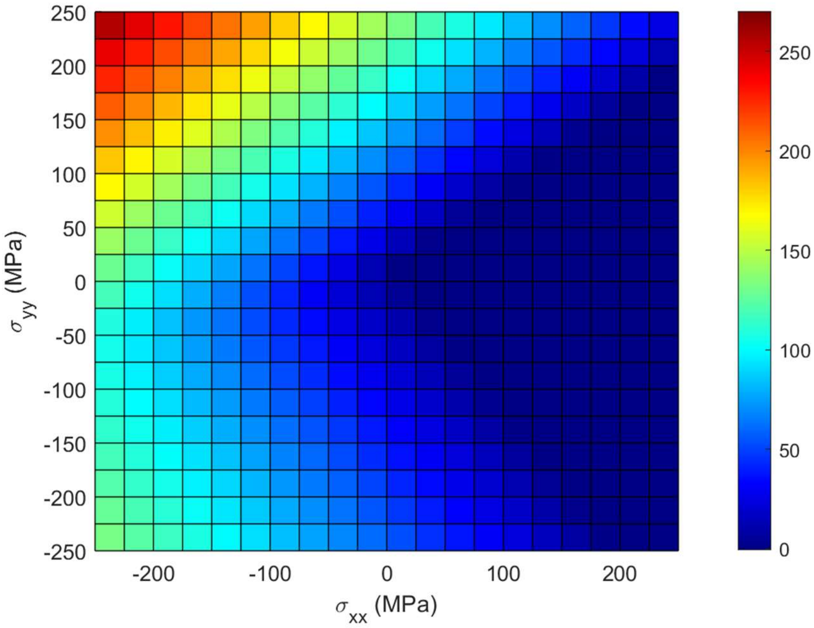

Fig. 1: Evolution of the predicted normalized H_{95}*: H at* $M = 0.95{\cdot}M_{sat}$, under biaxial stress states. The magnetic excitation and the magnetic sensors are along $\boldsymbol{x}$ (RD).

2 Conclusion

This work is a leap forward to understanding and modeling magnetization mechanisms for MBN interpretation. By combining the proposed simulation method's predictive capability with a new generation of magnetic sensors (local and directional), an ideal experimental configuration can be proposed particularly useful for workshop practice.

References

[1] Blitz, Jack. "Electrical and magnetic methods of non-destructive testing." *NASA STI/Recon Technical Report A* 94 (1991): 10775.S.K. Dwivedi et al., Materials Today: Proceedings, Vol. 5, Iss. 2, Part 1, pp. 3690-3698, 2018.

[2] Dwivedi, Sandeep Kumar, Manish Vishwakarma, and Akhilesh Soni. "Advances and researches on non destructive testing: A review." *Materials Today: Proceedings* 5.2 (2018): 3690-3698.

[3] Bertotti, Giorgio. *Hysteresis in magnetism: for physicists, materials scientists, and engineers*. Gulf Professional Publishing, 1998.

[4] Fagan, P., et al. "Multiscale modelling of the magnetic Barkhausen noise energy cycles." *Journal of Magnetism and Magnetic Materials* 517 (2021): 167395.

[5] Fagan, P., et al. "Magnetic Barkhausen noise: A simulation tool." *AIP Advances* 11.2 (2021): 025322.

[6] Hubert, Olivier, and Laurent Daniel. "Multiscale modeling of the magneto-mechanical behavior of grain-oriented silicon steels." *Journal of Magnetism and Magnetic Materials* 320.7 (2008): 1412-1422.